ENERGY HARVESTING FROM PIEZOELECTRIC STACKS VIA IMPACTING BEAM

A THESIS SUBMITTED TO
THE GRADUATE SCHOOL NATURAL AND APPLIED SCIENCES
OF
MIDDLE EAST TECHNICAL UNIVERSITY

BY

YİĞİT ÖZPAK

IN PARTIAL FULFILLMENT OF THE REQUIREMENTS
FOR
THE DEGREE OF MASTER OF SCIENCE
IN
MECHANICAL ENGINEERING

AUGUST 2014

Approval of the thesis:

ENERGY HARVESTING FROM PIEZOELECTRIC STACKS VIA IMPACTING BEAM

submitted by **YİĞİT ÖZPAK** in partial fulfillment of the requirements for the degree of **Master of Science in Mechanical Engineering Department, Middle East Technical University** by,

Prof. Dr. Canan Özgen _____
Dean, Graduate School of **Natural and Applied Sciences**

Prof. Dr. Suha Oral _____
Head of Department, **Mechanical Engineering**

Prof. Dr. Mehmet Çalışkan _____
Supervisor, **Mechanical Engineering Dept., METU**

Examining Committee Members:

Assist. Prof. Dr. Yiğit Yazıcıoğlu _____
Mechanical Engineering Dept., METU

Prof. Dr. H. Mehmet Çalışkan _____
Mechanical Engineering Dept., METU

Assoc. Prof. Dr. Ender Ciğeroğlu _____
Mechanical Engineering Dept., METU

Assist. Prof. Dr. Kıvanç Azgın _____
Mechanical Engineering Dept., METU

Dr. Murat Aykan _____
Design Leader, ASELSAN

Date: 29.08.2014

I hereby declare that all information in this document has been obtained and presented in accordance with academic rules and ethical conduct. I also declare that, as required by these rules and conduct, I have fully cited and referenced all material and results that are not original to this work.

Name, Last Name: Yiğit ÖZPAK

Signature :

ABSTRACT

ENERGY HARVESTING FROM PIEZOELECTRIC STACKS VIA IMPACTING BEAM

Özpak, Yiğit
M.S., Department of Mechanical Engineering
Supervisor: Prof. Dr. Mehmet Çalışkan

August 2014, 100 pages

Piezoelectric materials can be used for energy harvesting from ambient vibration due to their high power density and ease of application. Two basic methods, namely, tuning the natural frequency to the operational frequency and increasing the operation bandwidth of the harvester are commonly employed to maximize the energy harvested from piezoelectric materials. Majority of the studies performed in recent years focus mostly on tuning the natural frequency of the harvester. However, small deviations in operating frequency from the natural frequency can cause excessive loss in the power output. It is then advantageous to design a harvester which is capable operating in a wide frequency band. This goal could be achieved both by expanding effective bands of natural frequencies and introducing a frequency-rich external input to the system. The main idea is to supply constant excitation energy into the harvester system to obtain high energy levels by changing system characteristics. In this study, an analytical model of an impacting beam with piezoelectric stack at its tip is developed, in order to investigate the effects of

impacts on energy harvested. Experimental validation of analytical results is also performed.

Analytical expressions to obtain response of harvester and impact forces occurred during motion are generated for solution in MATLAB® platform by iterative solution methodology. Validation of the analytical model is performed upon comparisons with test results. Moreover, harvester efficiency for broadband frequency excitations is tested and its characteristic properties are investigated in detail.

Keywords: Piezoelectric Materials, Vibration Energy Harvesting, Experimental Validation, Impacting Beam, Structural Dynamics

ÖZ

ÇARPAN BİR KİRİŞTE PIEZOELEKTRIK MALZEME KULLANARAK ENERJİ HASADI

Özpak, Yiğit
Yüksek Lisans,Makina Mühendisliği Bölümü
Tez Yöneticisi : Prof. Dr. Mehmet Çalışkan

Ağustos 2014, 100 sayfa

Piezoelektrik malzemeler yüksek enerji yoğunluğu ve kullanım kolaylığından dolayı ortamdaki titreşimden enerji hasadında kullanılmaktadır. Hasatçının, doğal frekans değerini ayarlama ve operasyon bant aralığı artırma bu amaç doğrultusunda hasat edilen enerji miktarını maksimum yapmak için kullanılan iki ana yöntemdir. Son yıllarda yapılan çalışmalar genellikle hasatçının doğal frekans değerini ayarlamaya odaklanmaktadır. Fakat giriş değerinde oluşan doğal frekans değerinden ufak kaymalar, enerji çıkışında ciddi azalmalara sebep olmaktadır. Bu yüzden, geniş bantta çalışabilen hasatçı tasarımı daha avantajlıdır. Bu amaç, hem doğal frekans etkili bant aralığını arttırarak hem de sisteme dışarıdan frekansça zengin bir girdi sağlanarak başarılabilir. Ana düşünce, sistem karakteristiğini değiştirerek, sabit tahrik enerji altında hasatçının daha yüksek seviyelerde enerji çıktısını sağlamak. Bu çalışma da, çarpmanın enerji hasadı üzerinde ki etkilerini incelemek için, uç noktasında piezoelektrik yığına sahip çarpma altındaki kirişin analitik olarak modellenmesi geliştirilmiştir. Ayrıca, analitik sonuçların testlerde doğrulanması da gerçekleştirilmiştir.

Hareket sırasında, hasatçının tepkilerini ve oluşan çarpma kuvvetlerini bulmak için analitik ifadeler üretiliş olup, denklemler MATLAB® platformunda yinelemeli çözüm tekniği kullanılarak çözülmüştür. Analitik modelin doğrulanması testler ile sağlanmıştır. Bununla birlikte, hasatçının verimi geniş bantlı tahrikler ile test edilmiş ve karakteristik özellikleri detaylıca incelenmiştir.

Anahtar Kelimeler: Piezoelektrik Malzemeler, Piezoelektrik Malzemeler ile Enerji Hasadı, Deneysel Doğrulama, Çarpan Kiriş, Yapı Dinamiği

To My Family

ACKNOWLEDGEMENTS

I would like to extend my deepest gratitude to Prof. Dr. Mehmet ÇALIŞKAN for his help, guidance, advice, criticism and encouragements throughout the study.

I would like to thank Murat AYKAN of ASELSAN Inc. for supporting of my thesis and giving advices, suggestions throughout the study.

I would also like to thank Özge MENCEK of ASELSAN Inc. for sharing her comprehensive knowledge.

I am grateful to Kurtuluş ERSOY of ASELSAN Inc. for giving the idea studying in piezoelectric energy harvesting.

I am thankful to my company ASELSAN Inc. and to my colleagues, Furkan LÜLECİ, Anıl KOYUNCU, Taner KARAGÖZ, Fatih ALTUNEL, Elif ALTUNTOP, Kerim ÇEPNİ, Baran YILDIRIM, Serkan KAYILI, Tolga KÖKTÜRK and Ayşe Gözde ULU SOYSAL for supporting of my thesis and friendly office environment.

I owe special and deepest gratitude to my family Ezgi YILMAZ, Seyda ÖZPAK, Mustafa ÖZPAK, Abdullah Anıl ÖZPAK and Ayşe MIDIK for their friendship, love, support, patience and encouragement throughout the study.

TABLE OF CONTENTS

LIST OF TABLES

TABLES

LIST OF FIGURES

FIGURES

LIST OF SYMBOLS

E_b	Young modulus of the cantilever beam
I_b	Area moment of the inertia of a cantilever beam
A_b	Cross section of a cantilever beam
ρ_b	Density of the beam
m_b	Mass per unit length of the beam
L_b	Length of the beam
c_b	Damping coefficient of the beam
M_t	Mass of the tip mass
I_t	Mass moment of inertia of the tip mass
u_b	Base excitation displacement
$w(x,t)$	Steady-State Response of Cantilever Beam
E_s	Young modulus of the stopper
I_s	Area moment of the inertia of a stopper
A_s	Cross section of a stopper
ρ_s	Density of the stopper
m_s	Mass per unit length stopper
L_s	Length of the stopper
c_s	Damping coefficient of the stopper
$u(x,t)$	Steady-State response of Stopper
m_c	Compression mass of piezoelectric material
F_{pz}	Forcing function coming from compression mass to piezoelectric material
h_{pz}	Height of the piezoelectric material
m_{pz}	Mass per unit length of piezoelectric material
A_{pz}	Cross section of piezoelectric material

Y_{ij}	Young modulus of piezoelectric material
S_j	Strain produced in piezoelectric material
T_j	Stress produced in piezoelectric material
E_i	Electric field between piezo electrodes
D_i	Electrical displacement
g_{ij}	Piezoelectric voltage constant
d_{33}	Piezoelectric charge constant
V_{pz}	Voltage produced piezo
V_s	Voltage produced in stack
Q_{pz}	Charge produced piezo
Q_s	Charge produced in stack
C_{pz}	Capacitance of piezo
C_s	Capacitance of stack
$\varepsilon_{3,r}^{T}$	Permittivity of piezoelectric material for constant stress conditions
ε_0	Permittivity of free space
$\tan(\delta)$	Loss tangent property of stack
W_E	Harvested electrical energy
W_M	Transmitted mechanical Energy
$\ddot{b}(t)$	Base acceleration
ω	Operating frequency

Subscripts

r	Mode number
i	Direction of electric field
j	Direction of mechanical stress

Abbreviations

FFT	Fast Fourier Transformation
FRF	Frequency Response Function
PSD	Power Spectral Density

CHAPTER 1

INTRODUCTION

Energy harvesting from environmental sources has gained great attention in recent years. Common environmental sources exploited in energy harvesting can be listed as mechanical energy, thermal energy, light energy, electromagnetic energy, natural energy, human body, chemical and biological energies. For these kinds of energy conversions, there is no need to additional input to supply into system. The basic motivation is the conversion of the natural movements into electric charge. Adoption of a proper method for working conditions is the starting point of energy harvesting. For high power output in scale of kilowatts; solar, wave energy and wind could be used [1]. On the other hand; sources like mechanical vibration, radio frequency, inductive and light are more feasible ways of energy harvesting for the mili watt scale. Key components of harvesting energy consist of a transducer which converts energy into another form, such as piezoelectric material, and a medium to store the converted energy. Energy is conveniently converted into electrical form for the ease of storage.

In this thesis, mechanical vibration to electricity conversion mechanism is studied. Electromagnetic [2], electrostatic [3] and piezoelectric [5] means are the three main techniques of converting the available vibration energy to electricity.

Piezoelectric materials in mechanical-to-electrical energy conversion are very efficient means to supply energy needs for small electronic equipment. Great

majority of the machinery are exposed to vibration in working conditions. Consequently, with decreasing power needs of electronic cards used in such machinery, vibration based energy harvesting using piezoelectric materials becomes popular.

The main goal of this study is to maximize the power output of a harvester for the same amount of environmental vibration energy. Achievement of this goal is anticipated to expand the areas of use for piezoelectric materials, due to the increase in power output.

In the first chapter of the thesis, detailed information on energy harvesting and piezoelectricity phenomena are presented. In the second chapter, harvester models are reviewed with emphasis on their advantages and drawbacks. Studies on the enhancement of harvested power output are also summarized. In the third chapter, theoretical background of modelling of impacting beam problem is studied and an analytical model for the beam and its stopper is presented along with impact force calculations. Also, electromechanical modelling of piezoelectric stacks is performed. The fourth chapter includes validation of analytical results obtained in Chapter 3 with experimental data. In order to show the effects of impact on harvester frequency band, harmonic test results are shared in this part of study. In Chapter 5, main conclusions are drawn accompanied with discussion of the results. Future works on the subject are suggested in Chapter 6 to extend findings of this study.

In the following sections of this chapter brief information about piezoelectric energy conversion and basic methodologies are presented.

1.1 Energy Harvesting

Through advances in technology and decreases in power requirements of small electronic equipment, the idea of conversion of available environmental energy

in working systems is developed. Especially in powering electronic equipment, use of vibration energy to harvest mechanical energy into electric energy is very popular and useful. Piezoelectric materials have proven feasible as they have very high conversion efficiency due to their high power output and ease of application. Figure 1 is an explanatory visual to summarize this procedure.

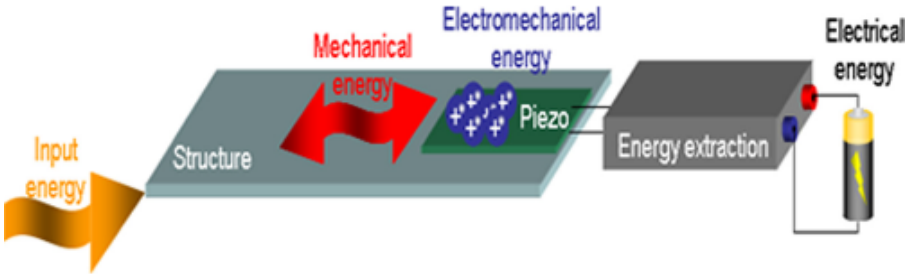

Figure 1. Schematic View of Mechanical Energy Conversion into Electric Energy Using Piezo[1]

In working conditions, mechanical movement of the structure results in kinetic energy. This energy can be converted into another form of energy by a process called as transduction performed by an appropriate transducer. For conversion of mechanical energy into electrical energy, piezoelectric material forms a very efficient transducer because of its chemical polarization. Applied force on such a material alters the strain leading to a change in the atomic structure of the initially polarized piezoelectric material. This results in the development of electric field as shown in Figure 2. Total voltage output depends on poling field voltage and thickness of the piezoelectric ceramic.

In sensor technology, this methodology is used to measure dynamic motion descriptors of the system such as acceleration and force levels. Moreover, due to decrease in power requirements of wireless sensor technology, this

methodology is also used to supply energy need of wireless sensor networks. In other words, same harvesting technology is used both to monitor the system changes and supply internal power requirements.

Piezoelectric mechanical resonators are very popular in military applications. Piezoelectric harvester devices are used to supply electrical energy to the electronic cards of smart munitions by converting kinetic energy occurring during the launch. Furthermore, they have long shell life and safety when compared to the chemical batteries not to mention reliability [6].

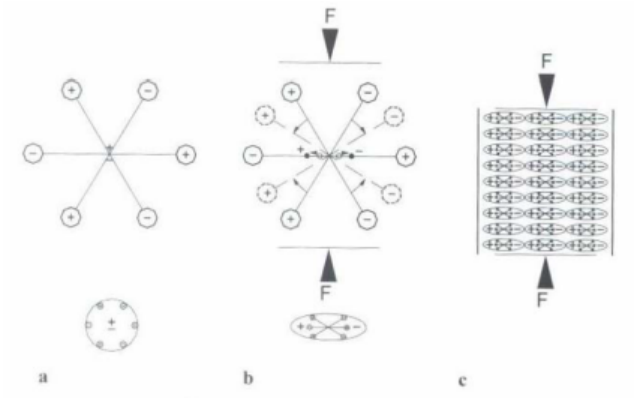

Figure 2. Polarization Process of a Piezoelectric Material[10]

1.2 Phenomenon of Piezoelectricity

The word ‘piezo’ originates from a Greek word meaning ‘to push’. Piezoelectricity should not be confused with ‘contact electricity’ (friction-generated static electricity or ‘pyroelectricity’, electricity generated from heating crystals). Piezoelectric materials produce charge when exposed to the

stress on its boundaries. This process can simply be summarized as a conversion of mechanical energy to electricity and called piezoelectricity.

Piezoelectric materials are composed of either crystals found in nature or ceramics and polymers manufactured artificially. Ceramics are more sensitive than crystals since their cutting direction and polarization can be tailored. Piezoelectric materials are also characterized according to easiness of polarization. If polarization of ceramic is easy, it is called as soft ceramic and if it is difficult to polarize, it is called hard. For high sensitivity applications soft ceramics should be used; however, for the high mechanical and electrical stress applications, hard doped ceramics are used. Initially, atomic structure of piezoelectric material is randomly dipoled and their polarization is adjusted by applying voltage and this polarization voltage determines the output voltage of material as shown in Figure 3 .

Piezoelectric materials are used for different loading and boundary conditions, which make them very popular in engineering applications. Moreover, their shapes are manufactured according to their areas of use.

In order to use piezoelectric materials in engineering applications, the mechanical to electrical energy conversion characteristics should be high to increase the efficiency of the conversion process. After 1950’s, production of the man-made piezo ceramics gained acceleration and their applications also increased on this reason.

As mentioned above, piezoelectric materials yield electric charge output when mechanically stressed and this is called direct piezoelectric effect. Curie brothers investigated this property in 1880. However, converse piezoelectric effect, by which mechanical motion can be obtained as a result of voltage

changes, is investigated by Gabriel Lippmann in 1881 [7]. Figure 4 shows schematic views of these two effects.

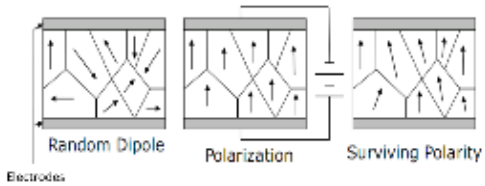

Figure 3. Polarization Process of Piezoelectric Material

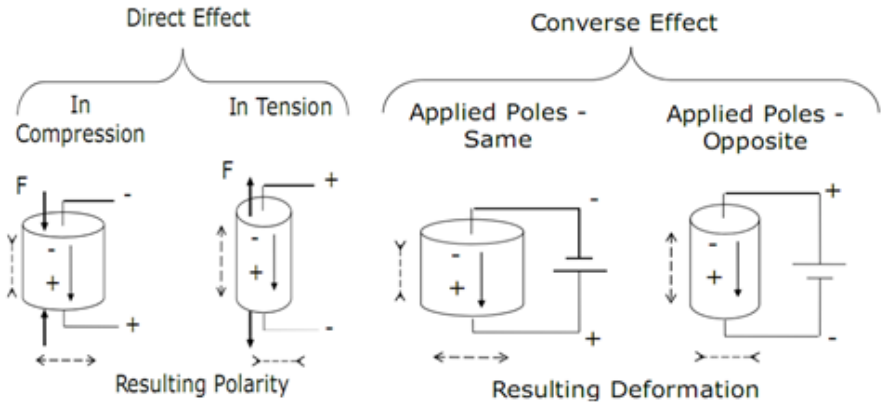

Figure 4. Direct and Converse Piezoelectric Effect [8]

Piezoelectric materials have very wide area of usage due to these direct and converse effects. Figure 5 summarizes the basic application areas based on the idea of piezoelectric effect.

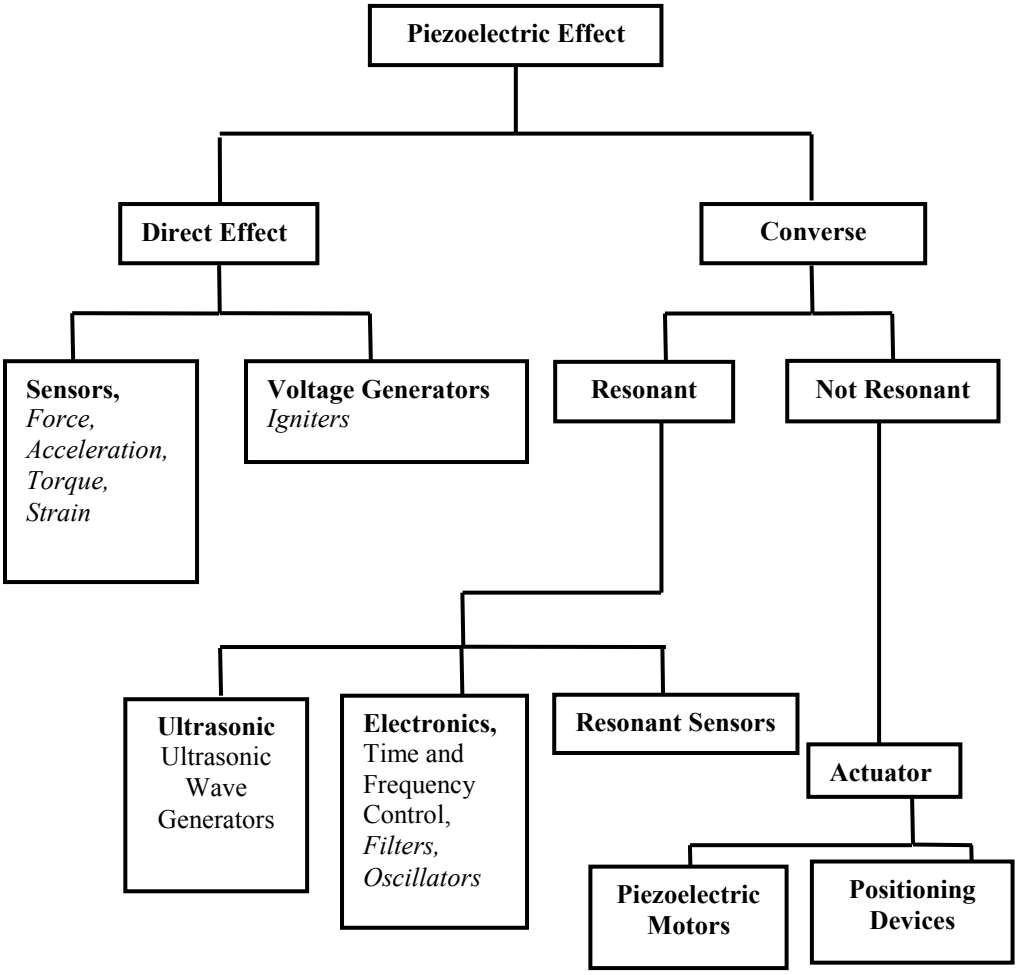

Figure 5. Application Areas of Piezoelectric Materials

Most of the properties of piezoelectric material depend on the direction and are generally designated as P_{ij} where P represents the material property, i represent the polarization direction or electric properties and j represents the force applied direction or mechanical properties. Therefore, in order to obtain accurate piezoelectric material model, direction information should be included in the modelling process. Figure 6 shows a detailed explanation and small example of direction assumptions.

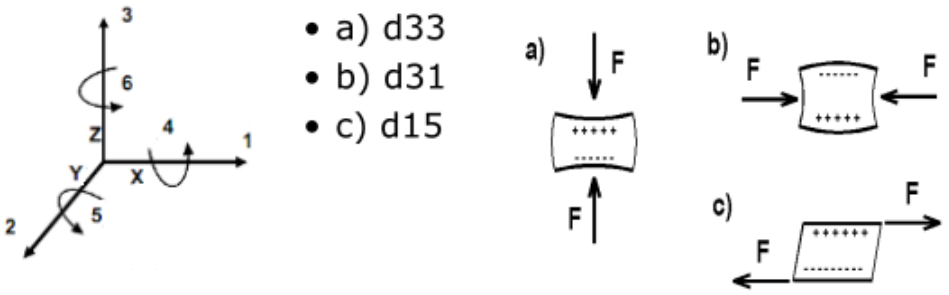

Figure 6. Piezoelectric Material Property Numbering Axis

1.3 Research Motivation and Objectives

In every part of engineering applications, decreasing power needs of systems has received great attention. This attention also has affected harvesting technologies and their importance has increased in recent years. In this area, piezoelectric materials have another advantage because their input comes from the default process of the system. There is no need to transport stored energy.

In literature, many studies are performed to model piezoelectric harvester and understand their mechanical (vibration) to electricity conversion. In recent years, different ways to increase power output capability are investigated and implemented. Generally, the power output of piezoelectric materials is increased by operating them at harvester's natural frequency. Figure 7 shows the voltage output characteristic of piezoelectric material when used at natural frequency and other frequencies.

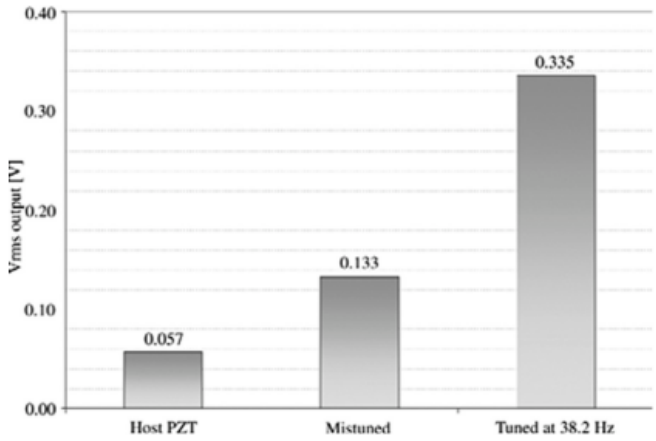

Figure 7. Output Voltage Representation for Tuned and Mistuned Frequencies [1]

However; tuning may not be possible for every harvester system or environment, especially for complex electronic equipment. Therefore, their efficiencies should be increased for broadband loading environments. This idea is the starting point of this study.

The main works performed in this thesis can be listed as follows:

- A detailed literature investigation for the current harvester models and their areas of use.
- Design of a harvester to obtain reasonable harvester efficiency over a wide frequency range.
- Analytical modelling of a proposed harvester along with piezoelectric stacks to predict mechanical and electrical responses.
- Experimental validation of analytical solution of the harvester and the piezoelectric material. Determination of the frequency band over which the harvester model is designed for high power outputs.
- Optimization study on harvester modelling by experimental data.

CHAPTER 2

LITERATURE SURVEY

Objective of this chapter is to present a thorough review of the studies on modelling of piezoelectric materials, especially piezoelectric stacks, and techniques to increase power output of piezoelectric materials. The advantages and drawbacks of already designed harvester systems and their harvester capabilities are discussed in detail.

2.1 Energy Harvesting Models Using Piezoelectric Material

Ersoy [9] aimed to investigate high power piezoelectric stacks and design a mechanical harvester to supply energy in munitions. In smart munitions, power requirements has decreased considerably over the last decades; therefore, he tried to provide this power by using piezoelectric stacks in firing a special type of munitions. In his study, he formed an analytical model to analyze material properties and design criteria. His harvester model is composed on compression mass and 25-layer piezoelectric stack. In analytical design part, firstly, he assumed piezoelectric stack bulk and force on each layer is equal. The electrical parameters are calculated based on this assumption. Then, as total force occurred on each layer is different, he used lumped parameter model in analytical harvester design. The comparison between these two analytical modelling is investigated and an accurate model is obtained. To show the accuracy of the analytical harvester model, he also modelled piezo in finite element tool ATILLA® and compared the analytical solution results with finite element outputs. In the last part of his work, to validate the results obtained from both analytical and finite element model, he designed different test

setups. In the first part of test section, he performed a harmonic (sweep sine) test using modal shaker and compared the solutions with analytical and numerical (finite element) results. He updated models upon comparisons of results and then to simulate munitions operation, impact hummer and pressure gun tests are concluded. The results at the end of whole work were reported to be consistent.

Pearson [10] performed a very similar study to Ersoy [9]. His aim was to supply required power to small electronic cards used in the munitions as a replacement alternative to chemical batteries. In his work, he tried to design a mechanical resonator model consisting of a mass and a spring. He tried to find out a simulation model which can be used to analyze energy harvesting efficiency and characteristic properties of piezoelectric material. He performed mechanical and electrical analyses on Simulink tool of MATLAB®. The output coming from these analyses was supplied into ORCAD PSCICE® to develop an equivalent circuit model of the piezo. In the experimental part, he used a 2 meter drop test setup which is very convenient way to simulate shooting of the munitions. Simulation results of analytical model and tests have displayed some differences. He concluded that techniques he used could be a good reference for the follow up works and some complementary studies should be performed.

Erturk [11] presented a detailed study to analyze coupled dynamics of a piezoelectric energy harvester. In his work, he used a beam like PZT to harvest energy. A distributed-parameter electromechanical model was used to predict dynamics of piezoelectric beam. Correction factors for the lumped parameter solutions were obtained from results obtained distributed- parameter solution. The analytical solution was compared to the results of different types of tests. In order to find the optimum load resistance using a single resistor and voltage measurement system, a simple experimental test setup was employed. Through

use of assumed-modes method, electromechanical models for Euler-Bernoulli, Rayleigh and Timoshenko models with axial deformations are investigated. In the last part of the study, a non-traditional energy harvester consisting of piezo, magneto and elastic effects was also offered. Additionally, sufficient number of energy harvester models covered in different studies was investigated.

2.2 Means to Maximize Harvested Energy

In the previous sections of this chapter, different means to model energy harvesters are investigated. Piezoelectric energy harvesters produce maximum output when operating frequency is equal to the natural frequency of the harvester system [1]. The reason of this phenomenon is that mechanical systems undergo largest motion amplitudes when excited at their natural frequency. In other words, piezo electric energy harvester is a resonant system that produces maximum power output when its resonant frequency matches the ambient vibration frequency. The deviation from the resonance causes significant decrease in power output. Mass and spring constants are effective parameters to control the resonant frequency of the system. The spring constant depends on material properties and dimensions of the material. Figure 8 shows the natural frequency calculation for the cantilever beam with tip mass to represent the effects of properties on the lowest harvester natural frequency.

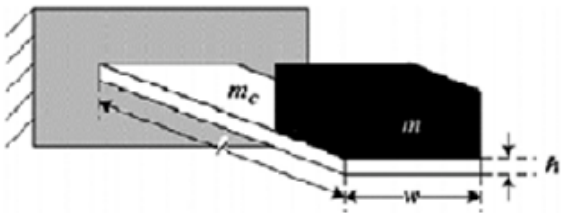

Figure 8. First Natural Frequency Calculation of One DOF assumption a Cantilever Beam [1]

Tuning the resonant frequency and increasing the operation bandwidth are two solutions to compensate the effects of frequency deviation. More detailed explanation of each solution is given below:

Means to increase harvested energy

- ***Frequency Tuning Methods***
  - ✓ Manual Frequency Tuning
    - ○ Mechanical Methods
      - Adding a tip mass
      - Moving center of gravity of harvester
      - Changing the dimensions
      - Changing the stiffness by axial preload
      - Changing the stiffness by extensional mode
    - ○ Magnetic Methods
    - ○ Electrical Methods
      - Changing the stiffness using piezoelectric actuator
      - Changing the capacitive load
  - ✓ Autonomous Frequency Tuning
- ***Increasing the Operation Frequency Bandwidth***
  - ✓ Random Vibration Sources

2.2.1 Frequency Tuning Methods

As mentioned in Section 1.1, piezoelectric materials yields the maximum voltage output, when ambient vibration frequency matches the energy harvester natural frequency. In literature, there are two main approaches to tune the

frequency of the harvester: manual and autonomous. Details of each one are presented in the upcoming sections.

2.2.1.1 Manual Frequency Tuning Methods

Manual frequency tuning methods are human dependent methods to harvest energy; in other words, external work should be done on system. Mechanical, magnetic and electrical means are the main methods for manual frequency tuning.

2.2.1.1.1 Mechanical Methods

The natural frequency of the harvester mainly depends on mass and stiffness operators. By applying external changes on these parameters, natural frequency can be changed in some range.

Cornwell *et al*. [12] change the natural frequency of the cantilever beam from 40.7 Hz to 38.2 Hz to match the base excitation frequency 38.2 Hz. Harvested voltage is demonstrated as increased from 0.133 V to 0.335 V in due course. This work clearly shows that exciting harvester at its natural frequency maximizes the electrical output variable.

Amongst other manual tuning methods, moving the center of gravity is used by Wu *et al*.[13]. In this study, the natural frequency of the harvester was changed by using movable point mass which was attached to a cantilever beam by a stud. Changing the location of the point mass, natural frequency is changed from 180 Hz to 130 Hz. Its harvester model is shown in Figure 9.

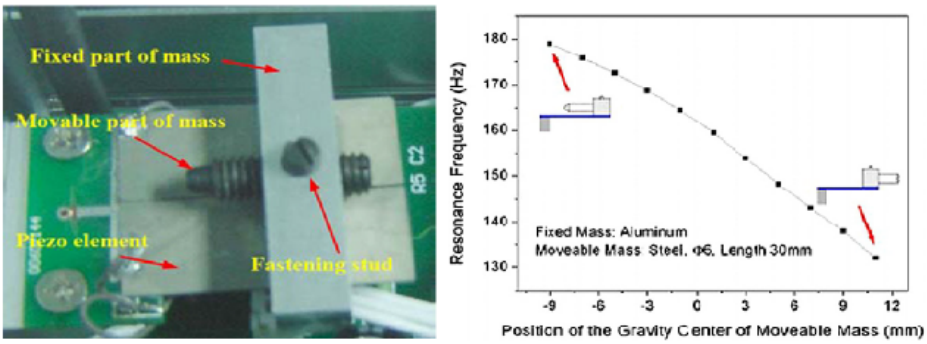

Figure 9. Effect of Moving Center of Gravity [13]

External force applied to the harvester changes the stiffness. In theory, natural frequency decreases when compressive force is applied; on the other hand, under tensile loading conditions, it should be increased [1]. Eichhorn *et al*. [14] show that it is possible to tune natural frequency about 26.19% under compressive force and about 4.44% under tensile force.

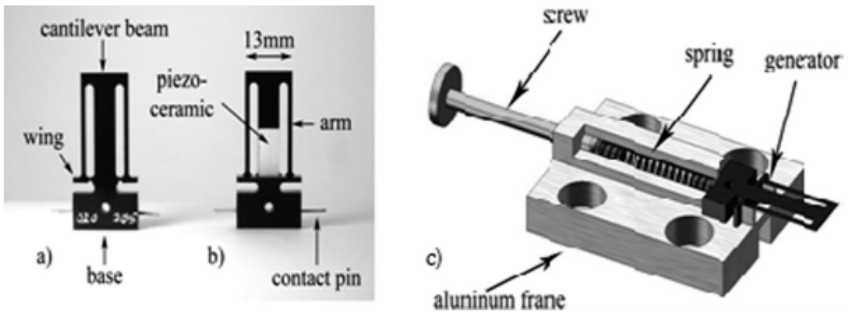

Figure 10. Energy harvester setup of Eichhorn *et al*. [14]

2.2.1.1.2 Magnetic Methods

Application of external force on energy harvester changes the stiffness as mentioned earlier. This is the basic idea magnetic methods lie on. Challa *et al*. [16] designed a harvester composed of a cantilever beam with tip mass and attractive and repulsive magnets at the end point as shown in Figure 11. Natural frequency was tuned between 22 Hz and 32 Hz by changing attractive force distance (d_a) and repulsive force distance (d_r). However, because of the damping effect introduced by such forces, power output efficiency could not be investigated accurately.

2.2.1.1.3 Electrical Methods

In magnetic and mechanical methods, electrical characteristics are predicted on stiffness change. Stiffness can be adjusted by changing dynamic properties such as geometrical moment of inertia using electrical voltage change. Similar work was accomplished by Peter *et al*.[18]. They designed a harvester system composed of an actuator and harvester beam piezo element illustrated in Figure 12. When the voltage is applied to the actuator, it changes the initial shape and consequently, geometrical moment of inertia changes. The harvester natural frequency was changed between 66 Hz and 89 Hz through such a method.

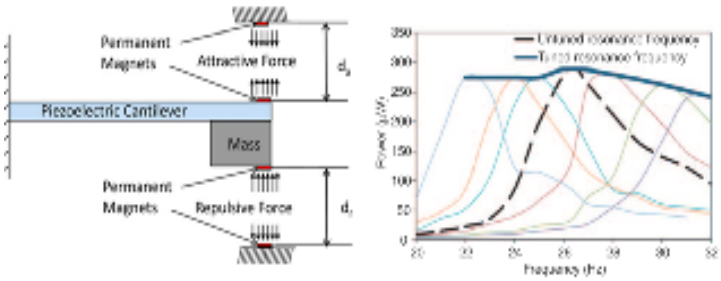

Figure 11. Tuneable Energy Harvester with Magnetic Method [16]

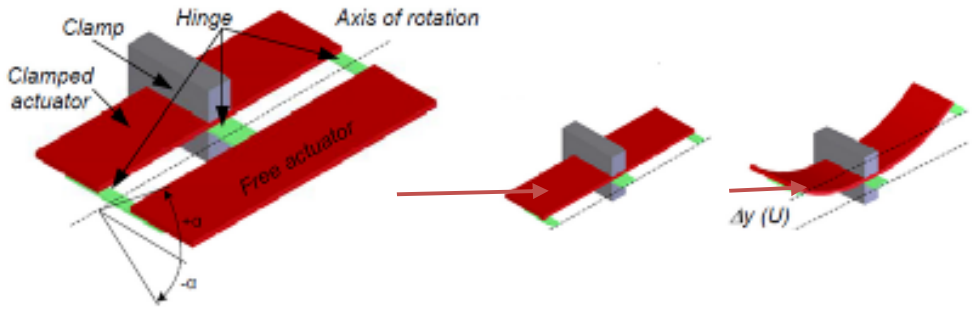

Figure 12: Energy Harvester Model of Peter *et al*. [18]

2.2.1.2 Autonomous Frequency Tuning

In manual frequency tuning methods, external changes should be supplied into the system to change the dynamic characteristic of the system. This is similar to finding an iterative solution of a mathematical problem. In contrast, in autonomous frequency tuning system makes these switches itself without any human interactions. These systems generally consist of sensors, amplifiers, controllers, harvester and other small electronic equipment. They monitor the system property in each step and control unit makes changes to tune harvester frequency with respect to an algorithm. Most important design criterion in autonomous frequency tuning is that the power spent to tune harvester should exceed harvested power. Therefore, while choosing electronic equipment, low power consuming types should be found and used. Otherwise the idea of harvester will conflict the design. Lallart *et al*. [19] studied on an autonomous tuning methods and schematic drawing of their design could be seen in Figure 13. The actuator embedded on the harvester can change the stiffness of the system as mentioned in electric methods.

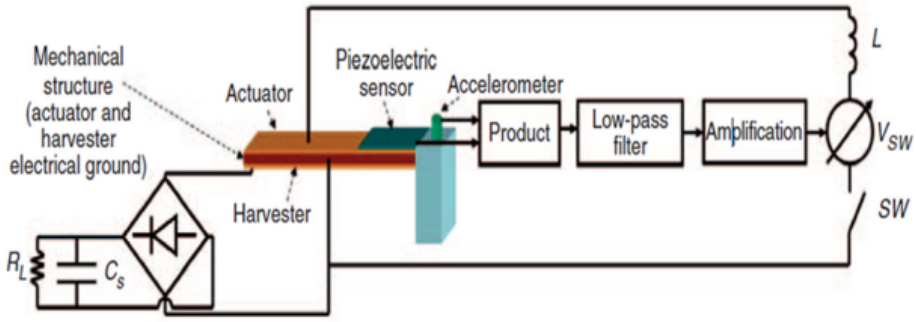

Figure 13. Autonomous Frequency Tuning Design by Lallart *et al*. [19]

2.2.2 Increasing Operation Frequency Bandwidth

Frequency tuning methods are briefly described earlier this chapter. Increasing the operation bandwidth is more complicated way compared to the other means of maximizing harvested energy. However, small deviations in the input frequency from the natural frequency can cause excessive decrease in the power output. Therefore, increasing the frequency bandwidth of the harvester enables the harvester to be used in broadband loading environments. There should be great differences between excitation frequency and natural frequency of the harvester and tuning could not be possible. Moreover, excitation frequency could not be a constant value; it could be a random source. In order to increase power output this kind of working conditions, if the harvester frequency bandwidth is increased, the efficiency of voltage production from piezoelectric materials is also increased. Therefore, this section of the chapter gives the brief information the ways could be used for this goal.

2.2.2.1 Random Vibration Sources

Additional excitation by a random vibration source can change operation bandwidth during motion of the harvester; in other words, harvester operation

frequency range includes environmental operation frequency and that of random vibration source. By this way, higher or lower modes are also shown up. Mak *et al*. [20] investigates this phenomenon by adding a stopper to a bimorph cantilever energy harvesting system as shown in Figure 14. In their work, harvester vibrates from base at first natural frequency located at 60 Hz. They added a stopper close to the tip mass location and due to base excitation; bimorph energy harvester impacts the stopper which cause excitation at the higher modes of the bimorph piezoelectric cantilever.

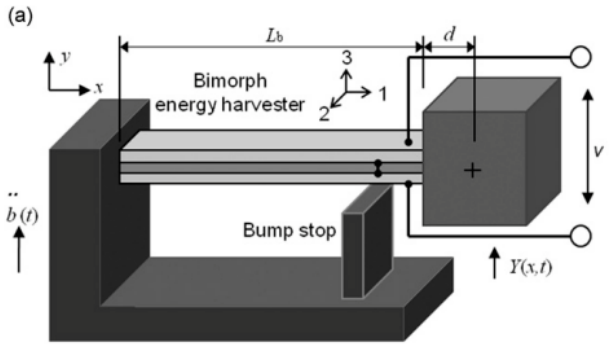

Figure 14. Sample Drawing of Harvester of Mak *et al*. [20]

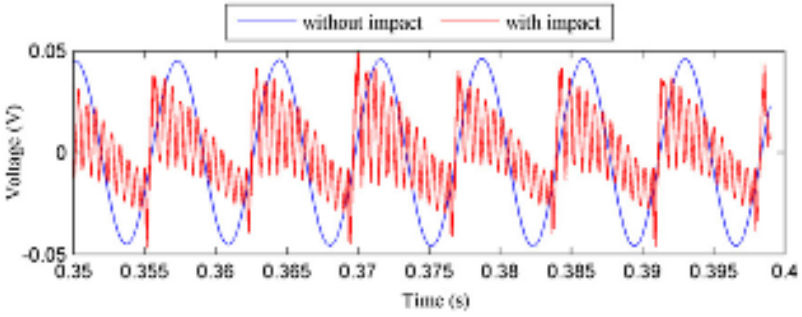

Figure 15. Voltage generation under the base motion, with stopper and without stopper [20]

2.3 Impacting Beam Problem

Impacting beam modelling is very complex study and in order to design an accurate model, as every numerical step should be analyzed. In engineering life, there are different examples of impact such as refrigerator compressor valves and engines [21].

In literature, there are two main approaches to model cantilever beam impact. These are Newtonian coefficient of restitution and numerical prediction of the impact force [20]. Advantages of Newton coefficient of restitution method is that it is simple to apply in solutions, does not require complex equations and has a wide range of examples. However, coefficient of restitution can change over short impact durations and it should be determined experimentally [20]. Moreover, to find effective mass of a cantilever impacting beam against stopper is another challenging drawback of this method. The second method involves prediction of impacting force between two bodies. This method requires a complex numerical procedure and difficult mathematical equations to solve come up since the responses of stopper and impacting beam should be solved simultaneously. The responses should be calculated in each step and the next step should be performed afterwards during the solution procedure.

Andrzej Rysak *et al*. [22] performed experimental studies to understand the dynamic behaviour of piezoelectric beam when subjected to impacts. According to their work, adding a stopper to system limits the vertical displacement and changes the stiffness of the beam. Therefore, their assumption is that there should be an increase in the harvester natural frequency accompanied with a reduction in response amplitude and efficiency of power output. They also shared that decreasing the gap size between the stopper and the beam increases the frequency bandwidth. Figure 16 displays their experimental results.

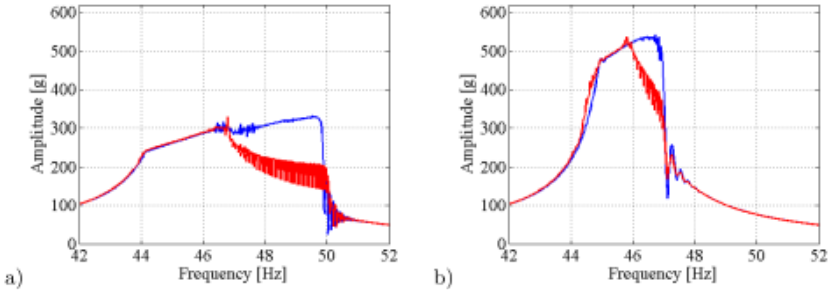

Figure 16. Andrzej Rysak *et al*. [22] Sweep Test Results. In Figure-a gap size is 6.5mm and in Figure-b gap size 11mm. Blue line shows up sweep and red line represent down sweep.

CHAPTER 3

THEORY

This chapter discusses analytical and numerical methods to model dynamic behaviour of a cantilever beam, its stopper and piezoelectric material placed on the beam. In the following sections, steady state response of the impacting cantilever beam, stopper and piezoelectric material under base excitation is analyzed. Lumped-parameter solutions are used to model each part individually. Coupled response equations are solved to find impact force between impacting beam and stopper. There are different types of solutions that could be used whose advantages and drawbacks are represented at impact solution part. In this study, a numerical solution procedure is adopted. This procedure comes with coupled equations and at each step of the solution, responses should be monitored to see whether the impacting process still continues or not. This part is the most challenging and difficult part of the theory as different parameters should be arranged together and convergence of the numerical solution should be check. In the section 3.6, electrical behaviour of piezoelectric material is discussed. The quasi-static solution procedure is used and equivalent circuit models are investigated to simplify the solution. Also, mathematical relations between single layer and multilayer piezoelectric material are discussed in detail. In the last part of the chapter, results of a case study are shared to represent analytical outcomes.

3.1 Base Excitation for the Transverse Vibration

In this section, distributed parameter solution is used to analyse the dynamic properties and response of the cantilever beam with tip mass under base

excitation. The Euler-Bernoulli beam with clamped-free boundary conditions is shown in Figure 17. Shear deformations and rotary inertia are neglected and cross sections are assumed to remain parallel.

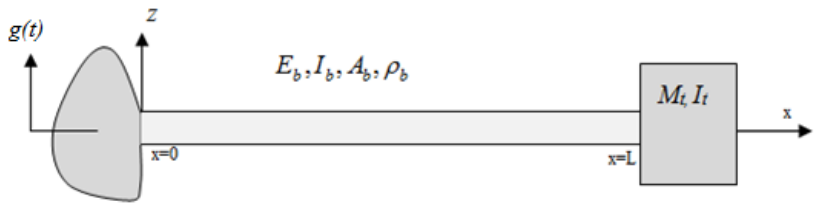

Figure 17. Clamped-Free Cantilever Beam under Base Excitation

Total response of the beam in transverse direction at any point and time is represented as *w(x,t)*. In Figure 17, *g(t)* is the base excitation value, E_b is the young modulus, I_b is the second moment of area, A_b is the cross section and ρ_b is the density of the beam. M_t is the mass and I_t is the mass moment of inertia of the tip mass at $x = L$. Equation of motion of an undamped Euler-Bernoulli beam can be obtained using Hamilton principle as follows:

$$\frac{\partial^2}{\partial x^2}(E_b I_b \frac{\partial^2 w(x,t)}{\partial x^2}) + \rho_b A_b \frac{\partial^2 w(x,t)}{\partial t^2} = 0 \qquad (3.1)$$

or

$$\frac{\partial^2}{\partial x^2}(E_b I_b \frac{\partial^2 w(x,t)}{\partial x^2}) + m_b \frac{\partial^2 w(x,t)}{\partial t^2} = 0 \qquad (3.2)$$

where m_b is the mass per unit length of a uniform isotropic cantilever beam.

The geometric boundary conditions for the clamped-free beam with tip mass at $x = 0$ are;

$$w(0,t) = 0 \qquad \frac{\partial w(0,t)}{\partial x} = 0 \tag{3.3}$$

The natural boundary conditions for the clamped-free beam with tip mass at $x = L$ are;

$$E_b I_b \frac{\partial^2 w(x,t)}{\partial x^2} + I_t \frac{\partial^3 w(x,t)}{\partial t^2 \partial x} = 0 \quad E_b I_b \frac{\partial^3 w(x,t)}{\partial x^3} - M_t \frac{\partial^2 w(x,t)}{\partial t^2} = 0 \tag{3.4}$$

The differential Equation (3.2) can be solved using separation of variables. Using expansion theorem, total response of the beam at any point and time can be expressed as,

$$w(x,t) = \sum_{r=1}^{\infty} \phi_r(x)\eta_r(t) \quad r = 1,2,... \tag{3.5}$$

where ϕ_r is the mass normalized mode shape function and η_r is the generalized coordinate of the r^{th} mode. For the any of the mode number, substitute Equation (3.5) into the Equation (3.2) and obtain Equation (1.6).

$$-\frac{1}{\eta(t)} \frac{\partial^2 \eta(t)}{\partial t^2} = \frac{1}{m_b \phi(x)} \frac{\partial^2}{\partial x^2} (\mathrm{E}_b I_b \frac{\partial^2 \phi(x)}{\partial x^2}) \tag{3.6}$$

In Equation (3.6) left and right hand sides of the equation depend on a different variable; therefore, both sides should be equal to a constant value for equality.

$$\frac{1}{\eta(t)} \frac{\partial^2 \eta(t)}{\partial t^2} = \lambda \tag{3.7}$$

$$\frac{1}{m\phi(x)} \frac{\partial^2}{\partial x^2} (\mathrm{E}_b I_b \frac{\partial^2 \phi(x)}{\partial x^2}) = -\lambda \tag{3.8}$$

Solution of the Equation (3.7) gives

$$\eta(t) = Ae^{\sqrt{\lambda}t} + Be^{-\sqrt{\lambda}t} \tag{3.9}$$

where A and B are arbitrary constants. If λ is positive $\eta(t)$ goes to infinity. However Equation (3.9) defines a physical system; therefore, λ should be a negative number.

$$\sqrt{\lambda} = i\omega \quad \text{where} \quad \lambda = -\omega^2 \tag{3.10}$$

Solution of Equation (3.8) yields a harmonic solution. The motion of any point on the beam is harmonic with frequency ω. Consider the spatial differential Equation (3.8) as

$$\frac{\partial^2}{\partial x^2}(\mathrm{E}_b I_b \frac{\partial^2 \phi(x)}{\partial x^2}) - \omega^2 m_b \phi(x) = 0 \tag{3.11}$$

$$\beta = \frac{\omega^2 m_b}{E_b I_b} \tag{3.12}$$

$$\frac{\partial^4 \phi(x)}{\partial x^4} - \beta \phi(x) = 0 \tag{3.13}$$

In order to solve Equation(3.13), four boundary conditions which are defined in Equation (3.3) and Equation (3.4) are needed. From the solution of Equation(3.13), natural frequency and mode shape functions of the system can be obtained. The solution of the fourth order homogeneous differential equation is expressed as

$$\phi_r(x) = A\cos(\frac{\beta_r}{L_b}x) + B\cosh(\frac{\beta_r}{L_b}x) + C\sin(\frac{\beta_r}{L_b}x) + D\sinh(\frac{\beta_r}{L_b}x) \quad \text{r=1,2,...} \tag{3.14}$$

where *A, B, C* and *D* are arbitrary constants. When boundary conditions given in Equation (3.3) and Equation (3.4) are substituted into the Equation (3.12), the solutions give:

$$A + B = 0 \tag{3.15}$$

$$C + D = 0 \tag{3.16}$$

After substitution Equation (3.15) into the Equation(3.14), mode shape function depends on *A* and *C* as follows

$$\phi_r(x) = A\left[\cos(\frac{\beta_r}{L_b}x) - \cosh(\frac{\beta_r}{L_b}x)\right] + C\left[\sin(\frac{\beta_r}{L_b}x) - \sinh(\frac{\beta_r}{L_b}x)\right] \quad r = 1,2,... \tag{3.17}$$

Substituting the remaining two boundary conditions given in Equation (3.4) into Equation (3.17);

$$\begin{pmatrix} \cos\beta_r + \cosh\beta_r - \frac{\beta_r^3 I_t}{m_b L_b^3}(\sin\beta_r + \sinh\beta_r) & \sin\beta_r + \sinh\beta_r + \frac{\beta_r^3 I_t}{m_b L_b^3}(\cos\beta_r - \cosh\beta_r) \\ \sin\beta_r - \sinh\beta_r - \frac{\beta_r M_t}{m_b L_b}(\cos\beta_r - \cosh\beta_r) & -\cos\beta_r - \cosh\beta_r + \frac{\beta_r M_t}{m_b L_b^3}(\sin\beta_r - \sinh\beta_r) \end{pmatrix} \begin{pmatrix} A \\ C \end{pmatrix} = \begin{pmatrix} 0 \\ 0 \end{pmatrix} \tag{3.18}$$

To obtain non-trivial solution from Equation(3.18), determinant of the coefficient matrix must be equal to zero.

$$\begin{aligned} &1 + \cos\beta_r \cosh\beta_r + \beta_r \frac{M_t}{m_b L_b}(\cos\beta_r \sinh\beta_r - \sin\beta_r \cosh\beta_r) \\ &-\frac{\beta_r^3 I_t}{m_b L^3}(\cosh\beta_r \sin\beta_r + \sinh\beta_r \cos\beta_r) + \frac{\beta_r^4 M_t I_t}{m^2{}_b L^4}(1 - \cos\beta_r \cosh\beta_r) = 0 \qquad r = 1,2,... \end{aligned} \tag{3.19}$$

Equation (3.19) is the characteristic equation of the differential equation of the Equation (3.11). The roots of this equation yield natural frequencies and mode shapes of the system. The undamped natural frequency expression for the r^{th} mode of the system is given by Equation(3.20).

$$\omega_{r=}\beta_r^{\,2}\sqrt{\frac{E_b I_b}{m_b L_b^{\,4}}} \quad r=1,2,... \tag{3.20}$$

and the corresponding mode shape function becomes :

$$\phi_r = A_r\left[\cos\frac{\beta_r}{L_b}x-\cosh\frac{\beta_r}{L_b}x+\varsigma_r\left(\sin\frac{\beta_r}{L_b}x-\sinh\frac{\beta_r}{L_b}x\right)\right] \quad r=1,2,... \tag{3.21}$$

where

$$\varsigma_r=\frac{\sin\beta_r-\sinh\beta_r+\beta_r\dfrac{M_t}{m_b L_b}(\cos\beta_r-\cosh\beta_r)}{\cos\beta_r+\cosh\beta_r-\beta_r\dfrac{M_t}{m_b L_b}(\sin\beta_r-\sinh\beta_r)} \quad r=1,2,... \tag{3.22}$$

In Equation (3.21) the mode shape function has arbitrary amplitude. Mode shape functions (Eigen functions) are unique, however amplitudes are changeable; therefore, to obtain unique amplitude and characteristic, mode shape functions are normalized. Equation (3.23) and Equation (3.24) show that normalization of mode shape functions [11] with tip mass as

$$\int\phi_s(x)m_b\phi_r(x)dx+\phi_s(x)\,\mathrm{M}_t\,\phi_r(x)+\left[\frac{d\phi_s(x)}{dx}+I_t\frac{d\phi_r(x)}{dx}\right]_{x=L}=0 \tag{3.23}$$

$$\int \phi_s(x) E_b I_b \frac{d^4\phi_r(x)}{dx^4} dx - \left[\phi_s(x) E_b I_b \frac{d^3\phi_r(x)}{dx^3} \right]_{x=L} + \ldots$$
$$\left[\frac{d\phi_s(x)}{dx} E_b I_b \frac{d^3\phi_r(x)}{dx^2} \right]_{x=L} = {w_r}^2 \delta_{rs} \qquad r,s = 1,2,\ldots \tag{3.24}$$

Using Equation (3.23) or Equation (3.24), arbitrary constant A_r can be found.

3.2 Response of Cantilever Beam under Base Excitation

Up to this section of the chapter, the damping effects of the structure are not included. Found mode shapes and natural frequencies are undamped. For the response of the beam, damping is a very important dynamic property. In order to include damping, the equation of motion can be modified as

$$\frac{\partial^2}{\partial x^2}(E_b I_b \frac{\partial^2 w(x,t)}{\partial x^2}) + c_b \frac{\partial w(x,t)}{\partial t} + m_b \frac{\partial^2 \mathrm{w(x,t)}}{\partial t^2} = -(m + M_t \delta(x-L)) \frac{d^2 u_b(t)}{dt^2} \tag{3.25}$$

In the forcing function damping effects and inertia of tip mass are neglected and tip mass effect is included directly in the modal function term where u_b is the base displacement. By using Equation (3.25), Equation (3.5) and orthogonality relations given in Equation (3.23) and (3.24), Equation (3.25) reduces to

$$\frac{d^2\eta_r(t)}{dt^2} + 2\zeta_r \omega_r \frac{d\eta_r(t)}{dt} + {\omega_r}^2 \eta_r(t) = f_r(\mathrm{t}) \tag{3.26}$$

where

$$f_r(t) = -\frac{d^2 u_b(t)}{dt^2}(m_b \textstyle\int_0^L \phi_r(x)dx + M_t \phi_r(\mathrm{L}_b)) \tag{3.27}$$

$$2\zeta_r \omega_r = \frac{c_b}{m_b} \tag{3.28}$$

Solution of the differential equation (3.26) can be obtained by using Duhamel integral for zero initial conditions [23]. Solution gives the modal response.

$$\eta_r(t) = \frac{1}{\omega_{rd}} \int_0^t f_r(\tau) e^{-\zeta_r \omega_r (t-\tau)} \sin \omega_{rd}(t-\tau) d\tau \quad r = 1, 2, \ldots \tag{3.29}$$

where ω_{rd} is damped natural frequency and defined as

$$\omega_{rd} = \omega_r \sqrt{1-\zeta^2} \quad r = 1, 2, \ldots \tag{3.30}$$

Total response can be found by multiplying modal coordinate given in Equation (3.29) with mode shape function given in Equation(3.21). After substituting Equation (3.29) into Equation(3.5), total response of the cantilever beam under base excitation and tip mass becomes

$$w(x,t) = \sum_{r=1}^{\infty} \frac{\phi_r(x)}{\omega_{rd}} \int_0^t f_r(\tau) e^{-\zeta_r \omega_r (t-\tau)} \sin \omega_{rd}(t-\tau) d\tau \quad r = 1, 2, \ldots \tag{3.31}$$

The solution given Equation (3.31) is only valid for the tip mass position at $x = L$. For any other position, response solution should be modified. Damping ratio assumptions must be correct to ensure the validity of the response amplitude. Damping ratios can be found by using two modes; however the best way to find damping ratios is, to perform experiments at each mode and obtain the ratio for that mode. In section 4.1 experimental results for damping values of cantilever beam are given.

3.3 Longitudinal Vibration of the Stopper Bar

In the previous section, transverse vibration of a cantilever beam with tip mass under base excitation has been analysed and steady state response has been obtained. In this section, the longitudinal vibration of a bar to serve as the stopper is discussed. In the impacting force calculations, the coupled dynamic equations of the beam and the stopper should be solved. The beam and stopper stand on the same base; therefore, while the beam undergoes transverse motion, the stopper executes longitudinal/axial motion. The procedure used to model stopper motion is very similar to that of transverse vibration of beam given in the previous section. Figure 18 shows the schematic drawing of the stopper.

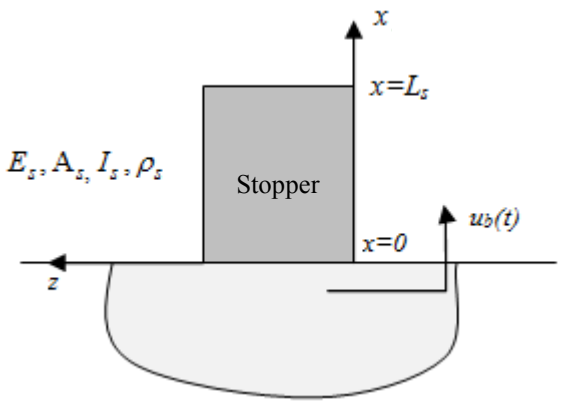

Figure 18: Fixed- Free Bar under Base Excitation

The beam is subjected to displacement input from the base and vibrates in x direction shown with $u_b(t)$ in Figure 18. Here, E_s is the Young's modulus, A_s is the cross-section area, ρ_s is the material density and I_s is the second moment of area of the bar which is used as a stopper in the harvester system. m_s stands for

mass per unit length of the bar in the following equations. In response calculation of , some steps are not mentioned as the solution of differential equations is the same with transverse vibration of the beam. The equation of motion for the undamped free vibration of a bar in axial direction is defined as:

$$E_s A_s \frac{\partial^2 u(x,t)}{\partial t^2} - m_s \frac{\partial^2 u(x,t)}{\partial t^2} = 0 \tag{3.32}$$

Total response of the stopper is the summation of multiplication of mode shapes and generalized coordinates of all modes as given in Equation(3.33).

$$u(x,t) = \sum_{r=1}^{\infty} \phi_r \eta_r \quad r = 1,2,... \tag{3.33}$$

Using separation of variables, ordinary differential equations can be obtained and their solution gives characteristic equation for each mode shape as follows:

$$\cos \beta_r L_s = 0 \quad r = 1,2,... \tag{3.34}$$

Solution of characteristic equation gives the roots or β_r :

$$\beta_r = (2r-1)\frac{\pi}{2L_s} \quad r = 1,2,... \tag{3.35}$$

From Equation(3.35), undamped natural frequencies and the mode shape functions can be obtained as given in Equation(3.36) and Equation(3.37), respectively:

$$w_r = \beta_r \sqrt{\frac{E_s I_s}{m_s}} \quad r = 1,2,... \tag{3.36}$$

$$\phi_r(x) = A_r \sin \beta_r x \quad r = 1, 2, \ldots \tag{3.37}$$

Given mode shape function in Equation (3.37) is unique; however, using mass normalization function, its amplitude also becomes unique.

$$\int \phi_s(x) m_s \phi_r(x) dx = 1 \quad \text{for } r \neq s \quad r, s = 1, 2, \ldots \tag{3.38}$$

Using Equation (3.38) arbitrary constant A_r can be found as $\sqrt{\frac{2}{m_s L_s}}$.

As mentioned earlier, differential equations governing longitudinal vibration are very similar to that of transverse vibrations. Substituting Equation (3.33) into Equation (3.32), then multiplying with $\phi_r(x)$ and integrating over the length of the stopper, generalized damped modal response expression becomes:

$$\eta_r(t) = \frac{1}{\omega_{rd}} \int_0^t f_r(\tau) e^{-\zeta_r \omega_r (t-\tau)} \sin \omega_{rd} (t-\tau) d\tau \quad r = 1, 2, \ldots \tag{3.39}$$

And total response can be written as

$$u(x,t) = \sum_{r=1}^{\infty} \frac{\phi_r(x)}{\omega_{rd}} \int_0^t f_r(\tau) e^{-\zeta_r \omega_r (t-\tau)} \sin \omega_{rd} (t-\tau) d\tau \quad r = 1, 2, \ldots \tag{3.40}$$

Where model forcing function $f_r(t)$ is

$$f_r(t) = -\frac{d^2 u_b(t)}{dt^2} m \int_0^{L_S} \phi_r(x) dx \quad r = 1, 2, \ldots \tag{3.41}$$

The time response of the stopper at any point can be found by Equation (3.40). In this model of the stopper, tip mass equations or corrections are not used.

However, by following transverse vibration part, these effects can be inserted into the equations using same procedure.

3.4 Solutions of Impacting Problem and Force Calculation

In literature, different types of solutions to an impacting beam problem are available. Impact force is the main requirement to obtain the total response of both impacting beam and stopper. The total force depends on the material properties, initial gap, crossing point, crossing area and base acceleration level. Crossing point and crossing area represent the location of impact between the stopper and the cantilever beam and the impact area between two bodies. Figure 19 shows a schematic view of the impacting beam problem and initial gap is the distance between two bodies at rest.

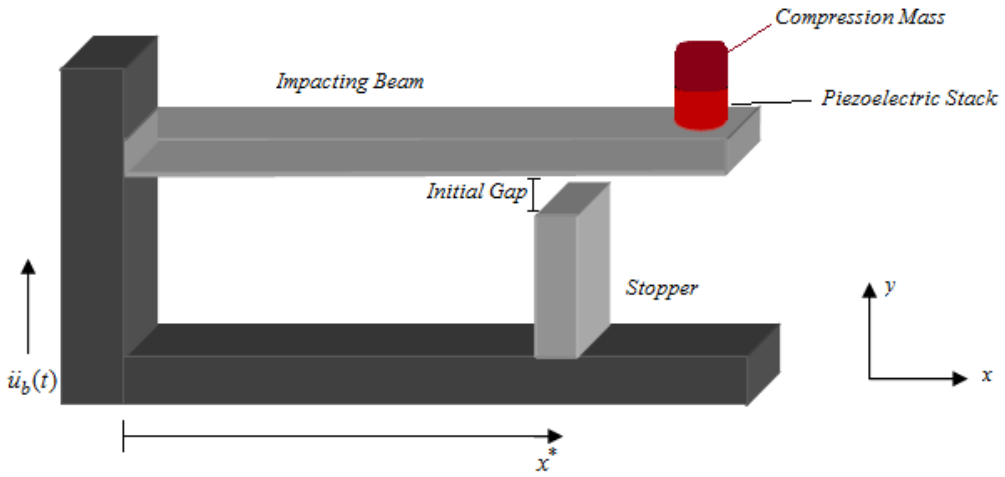

Figure 19: Impacting Beam Problem

There are three basic and illustrated solution methods commonly used in literature. First one is the coefficient of restitution method. Generally, this method is commonly used in impacting problems. The formulation and procedure is relatively simple and steady. Specific experiments should be performed to find exact coefficient. The contact duration in every step should be determined carefully, as changes in the contact duration cause higher modes to be excited [20]. The other drawback is the necessity of effective impact determination. For these reasons the coefficient of restitution method is not recommended for beam-like structures [20]. The second one is Hertzian contact method to find contact force. This is useful way if two bodies are comparable in size and contact duration is relatively long [21]. The third method is a numerical method with the main idea of modelling both systems as continuous and solving the coupled equations for displacements. For such kind of simple structures it is easy to obtain the contact force. On the other hand, the method has certain drawbacks such as the complexity of the coupled equations and sensitivity of the chosen solution time step considering number of modes employed in the solution. Furthermore, solution time takes longer when compared to the other methods because of the numerical integration involved. Higher frequency modes can also be considered during impact. In following parts, convergence studies are performed to determine the number of modes and the appropriate time step.

A very important point for impacting beam studies is that; the harvester power output increases with increasing base acceleration level, whereas the fatigue life decreases. Therefore during modelling and testing of this kind of structures, this issue should be considered.

Figure 20 shows the schematic drawing of impacting beam system and x^* shows the impact location, Δ represent the initial gap or distance between bodies before motion is imparted.

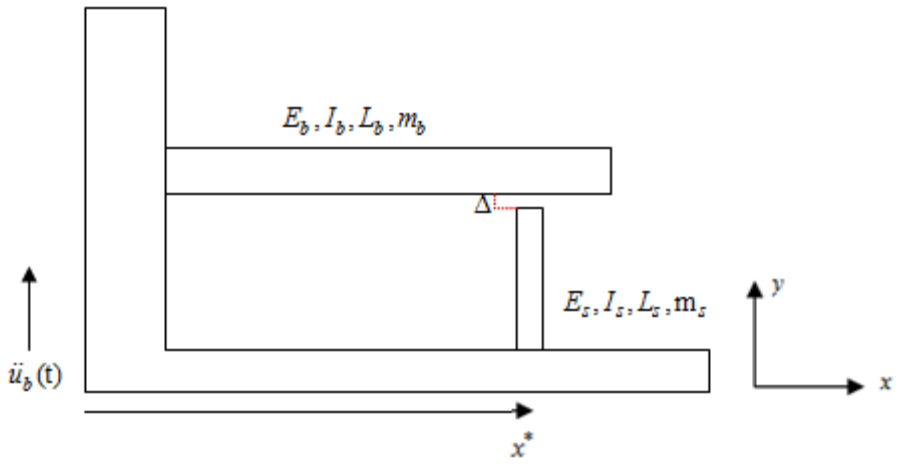

Figure 20: Schematic Drawing of Impacting Beam System

When the base starts to accelerate, both the beam and stopper moves together, and give different responses at each frequency. Maximum response can be obtained monitoring the beam when the excitation frequency gets closest to its natural frequency. At frequencies close to the natural frequency of the beam, the gap Δ decreases. When $\Delta > 0$, there is no contact between impacting beam and stopper and they move separately with the base excitation. Responses can be obtained by the equations given in sections 3.1 and 3.2. When $\Delta = 0$, impact occurs. The beam and stopper are subjected to both base excitation and positive impact force. In numerical calculations it is observed that during the impact, total impact force is positive and after the separation impact force becomes negative. This is the basic approach used to monitor whether contact still continues or not. The impact force is assumed as a point force and the total impact force is the summation of point forces. Total response of the beam and stopper can be expressed as described below.

Beam motion during impact:

$$w(\mathrm{x},\mathrm{t}) = \mathrm{w}_b(x,t) + w_{imp}(x,t) \tag{3.42}$$

$$w(\mathrm{x},\mathrm{t}) = \mathrm{w}_b(x,t) + \int_0^t g_b(x,t-\tau)F(\tau)d\tau \tag{3.43}$$

where $w(x,t)$ total response of the beam, $w_b(x,t)$ is the response coming from base acceleration, $g_b(x,t)$ is unit impulse response function and $F(t)$ is the impact force. The stopper motion during the impact:

$$u(y,t) = u_b(y,t) - u_{imp}(\mathrm{y},\mathrm{t}) \tag{3.44}$$

$$u(y,t) = u_b(y,t) - \int_0^t g_s(y,t-\tau)F(\tau)d\tau \tag{3.45}$$

where $u(y,t)$ is total response of the stopper, $u_b(y,t)$ is the response coming from base acceleration, $g_s(y,t)$ is unit impulse response function and $F(t)$ is the impact force.

The contact positions and times can be found by the solution of the Equation (3.46)

$$w(x^*,t) = u(L_s,t) - \Delta \tag{3.46}$$

where Δ is a positive value for this coordinate system convention adopted.

Unit impulse response functions can be defined for the n^{th} mode when the force is applied to beam at $x = x^*$ and to the stopper at $y = L_s$ as follows [24]:

$$g_b(x,t)=\sum_{r=1}^{n_b}\frac{\phi_{br}(x)}{m_b w_{db}}\phi_{br}(x^*)\,\mathrm{e}^{-\zeta_{br}w_{nbr}t}\sin(w_{db}t)\quad r=1,2,... \tag{3.47}$$

$$g_s(y,\mathrm{t})=\sum_{r=1}^{n_b}\frac{\phi_{sr}(\mathrm{y})}{m_s w_{ds}}\phi_{sr}(L_s)\,\mathrm{e}^{-\zeta_{sr}w_{nsr}t}\sin(w_{ds}t)\quad r=1,2,... \tag{3.48}$$

Equilibrium point can be found from Equation (3.49)

$$\mathrm{w}_b(x^*,t)+\int_0^t g_b(x^*,t-\tau)F(\tau)d\tau=u_b(\mathrm{L}_s,t)-\int_0^t g_s(\mathrm{L}_s,t-\tau)F(\tau)d\tau-\Delta \tag{3.49}$$

However, in Equation (3.49) impact force *F(t)* is not known. Rearranging Equation (3.49) the integration can be divided in two parts.

$$\int_0^t g_b(x^*,t-\tau)F(\tau)d\tau=\int_0^{t-\Delta t} g_b(x^*,t-\tau)F(\tau)d\tau+\int_{t-\Delta t}^t g_b(x^*,t-\tau)F(\tau)d\tau \tag{3.50}$$

$$\int_0^t g_s(\mathrm{L}_s,t-\tau)F(\tau)d\tau=\int_0^{t-\Delta t} g_s(\mathrm{L}_s,t-\tau)F(\tau)d\tau+\int_{t-\Delta t}^t g_s(\mathrm{L}_s,t-\tau)F(\tau)d\tau \tag{3.51}$$

Δt is defined as the very small fixed time step to solve one part of integration with area calculation. Rearranging Equation (3.50) and (3.51) as:

$$\int_0^t g_b(x^*,t-\tau)F(\tau)d\tau=\int_0^{t-\Delta t} g_b(x^*,t-\tau)F(\tau)d\tau+g_b(x^*,t-\tau)F(\tau)\Delta\mathrm{t} \tag{3.52}$$

$$\int_0^t g_s(\mathrm{L}_s,t-\tau)F(\tau)d\tau=\int_0^{t-\Delta t} g_s(\mathrm{L}_s,t-\tau)F(\tau)d\tau+g_s(\mathrm{L}_s,t-\tau)F(\tau)\Delta\mathrm{t} \tag{3.53}$$

Inserting Equation (3.52) and Equation (3.53) into the Equation (3.49); Equation (3.54) is obtained which is the equilibrium of motion of beam and stopper. The reason of these modifications is to remove the one force term out from the integration to go on with numeric iteration solution.

$$\mathrm{w}_b(x^*,t)+\int_0^{t-\Delta t} g_b(x^*,t-\tau)F(\tau)d\tau+g_b(x^*,t-\tau)F(\tau)\Delta t=u_b(\mathrm{L}_s,t)-\int_0^{t-\Delta t} g_s(\mathrm{L}_s,t-\tau)F(\tau)d\tau-g_s(\mathrm{L}_s,t-\tau)F(\tau)\Delta\,\mathrm{t}-\Delta \tag{3.54}$$

Using Equation (3.54) and introducing S1, S2 and S3 the following relations are obtained.

$$S_1=\mathrm{w}_b(x^*,t)+\int_0^{t-\Delta t} g_b(x^*,t-\tau)F(\tau)d\tau \tag{3.55}$$

$$S_2=u_b(\mathrm{L}_s,t)-\int_0^{t-\Delta t} g_s(\mathrm{L}_s,t-\tau)F(\tau)d\tau \tag{3.56}$$

$$S_3=g_b(x^*,t-\tau)\Delta t+g_s(L_s,t-\tau)\Delta t \tag{3.57}$$

Total impact force could be defined as by Equation(3.58)

$$F(t)=-\frac{S_1-S_2+\Delta}{S_3} \tag{3.58}$$

When the impact occurs, crossing point location of beam is below the stopper impact point, otherwise above the location of stopper. Mathematical representations are outlined as:

$$w(x^*,t)\le u(L_s,t)-\Delta \tag{3.59}$$

$$F(t)\ge 0 \tag{3.60}$$

When there is no contact,

$$w(x^*,t)\ge u(L_s,t)-\Delta \tag{3.61}$$

$$F(t)\le 0 \tag{3.62}$$

In numerical solution case, contact force should be controlled in every step and if it is positive, it means two bodies are still in contact and otherwise separated. In this kind of solutions, time step should be chosen carefully to ensure the convergence of the solution. If it is too small, numerical solution time becomes very long and solution may diverge. If it is too large, contact may not occur and high frequency harmonics cannot be monitored. To find suitable time step, some convergence studies have been done. Fathi *et al*. suggest that time step must be at least twice the period of highest mode [29]. The whole procedure is drawn in Figure 21 as a flowchart to define control loop easily.

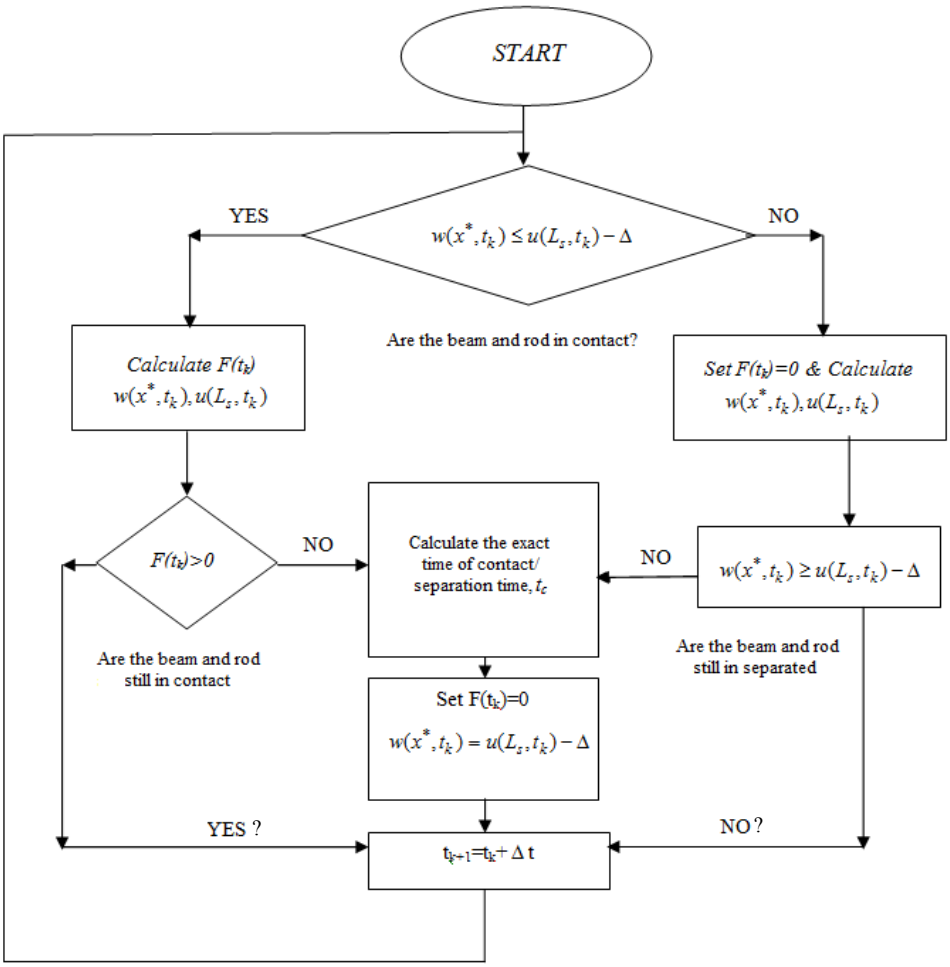

Figure 21: Schematic flowchart of numerical implementation of impact model

3.5 The Convolution Sum

Dynamic behaviour of continuous systems can be approximated by discrete system equations and be solved numerically on computers. Response of a beam under arbitrary forces could be solved by using convolution integral; however, it could be difficult to express the force function in a simple form. Therefore, the solution of convolution integral becomes troublesome. Figure 22 shows a discretization of a force signal. In this way, complicated force function responses are solved by convolution sum instead of integration. Figure 23 shows the analogy chart of the discretization of time signal and response calculation. During the impact, each time step gives different force, therefore defining force as a function is very difficult. As mentioned, calculated impact force is monitored in each step. Impact force at each step causes a response not only at that step but also at the next steps. Therefore, the response caused by impact at each step is calculated throughout the whole excitation duration. As a result, a set of responses are obtained for each impact force from each step. These sets can be summed to obtain the total response. In other words, total response coming from repetitive and constant time step impacts is the summation of each individual impact force response and its effects on whole time. This is well known as the convolution sum.

Discrete time excitation of force signal shown in Figure 22 is can be written as:

$$F(n) = \sum_{k=0}^{\infty} F(k)\delta(n-k) \tag{3.63}$$

$$x(n) = \sum_{k=0}^{n} F(k)g(n-k) \tag{3.64}$$

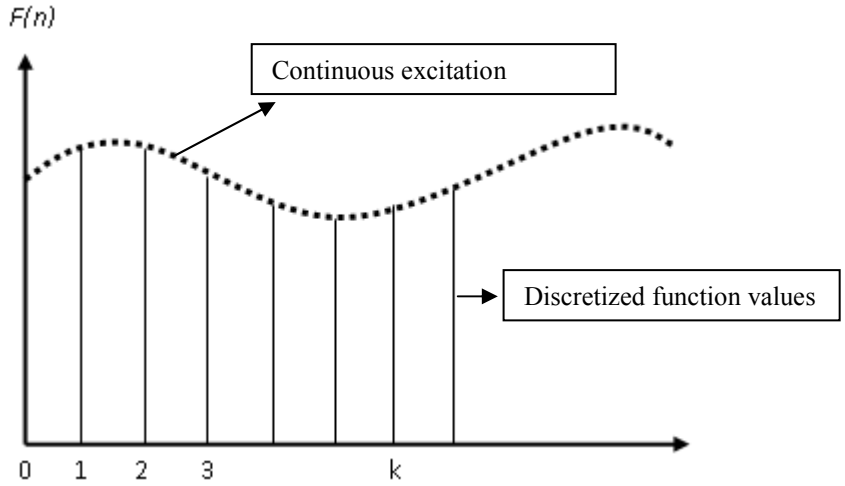

Figure 22: Discrete Time Excitation Function [23]

x(n) is the summation of the responses obtained for discrete force signal *F(n)* where *n* is the discretization of time and force signal or solution time step of the discrete system, *g(n)* is the unit impulse response of a discrete signal for zero initial conditions.

The theory of impulse response implies that $g(n)=0$ for $n<0$, since the system is at rest before the force is applied. In every time step $n>0$ effects of the force signal happened before are included in the response at that time.

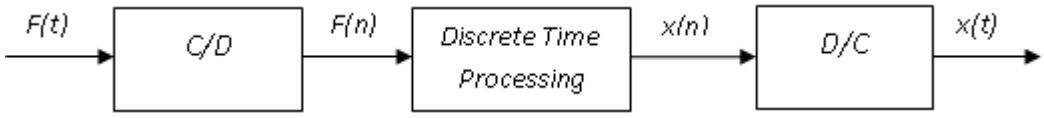

Figure 23: Schematic chart for algorithm of convolution sum

Response can be obtained after any arbitrary number of time steps as follows:

$$x(n) = \sum_{k=0}^{n_0} F(k)g(n-k) \tag{3.65}$$

where n_0 is the number of time steps used in force signal discretization procedure up to that time instant; however, n is independent from n_0 and can be increased according to the sought time response caused by impact even after the force application is over. Total response is obtained once n_0 is large enough to cover the force implementation.

3.6 Modelling Piezoelectric Stacks

There exist different ways to model different piezoelectric materials. In this thesis cylindrical multilayer piezoelectric materials (Figure 24) having high power density are used. It is also an electro-mechanical modelling study therefore the relations between electrical and mechanical properties should be investigated to design the most efficient system.

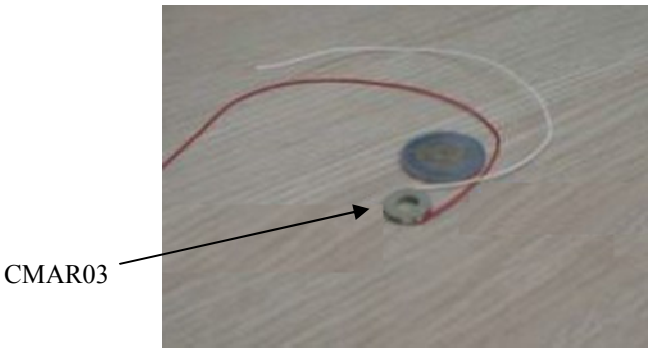

Figure 24: CMAR03 Piezoelectric Material

As mentioned earlier, strain changes in the piezoelectric materials result in voltage output. To model piezoelectric stacks and obtain strain changes, different mechanical modelling techniques and assumptions could be used. However, each method has its advantages and drawbacks such as easiness and accuracy. These assumptions are also valid for the compression mass modelling. The first approach for the piezo ceramic modelling in this thesis is the assumption of piezoelectric material as rigid and calculating electric output by simply using compression force and electric equations [9]. The second approach involves modelling piezo material as a continuous structure and adding effects of each layer to the output; in other words, calculation of force and electric output for each layer. The comparisons of these two approaches are given in the next section and results chapter.

For the electrical modelling part, the relation between the strain and voltage, the effects of high power density stacks for this kind of energy harvesting problems are investigated.

3.6.1 Mechanical Modelling of Piezoelectric Stacks

In this thesis piezo and compression mass are bolted to the cantilever beam from its end; therefore, tip mass of the beam consists of piezo, compression mass, bolt and washer. Figure 25 shows the cross-section of this configuration.

During the motion of the base where piezo and compression mass are inserted, the total force on the piezo could be calculated from Newton 2nd law as

$$F_{pz} = m_c \ddot{b}(t) \tag{3.66}$$

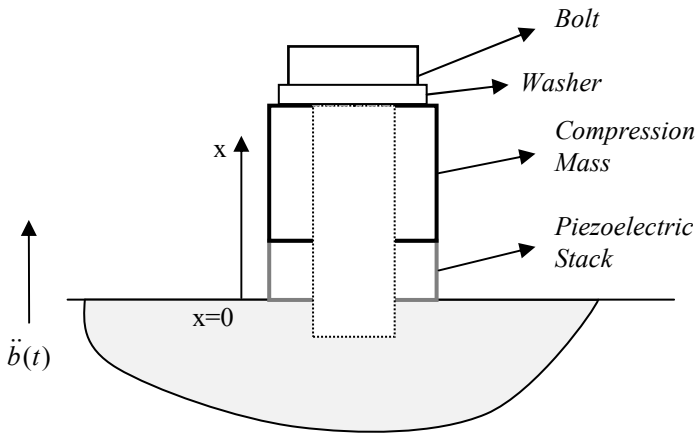

Figure 25: Compression Mass Model of Piezoelectric Material

where F_{pz} is the total force, m_c is compression mass, $\ddot{b}(t)$ base acceleration. The strain formed on each layer of piezo should be calculated by distributed parameter modelling.

Piezoelectric material given in Figure 26 is composed of n layers and each layer has a capability to produce voltage output individually.

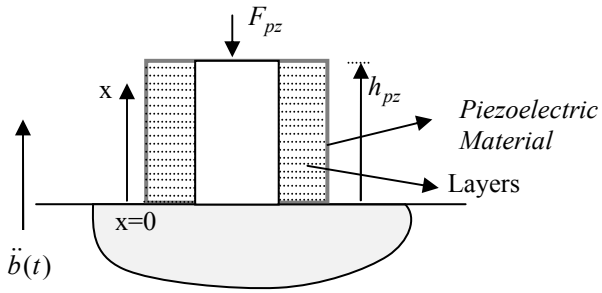

Figure 26: Detailed View of Piezoelectric Material

The example drawing of piezo stack is illustrated in Figure 27 to show the layer settlement. Each layer is composed of PZT ceramic and internal electrodes.

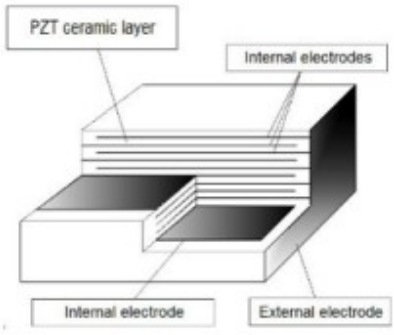

Figure 27: Piezoelectric Stack Cross Section [25]

The equation of motion of the piezoelectric material can be written as

$$\frac{\partial}{\partial x}\left[Y_{ij} A_{pz}(x) \frac{\partial u(x,t)}{\partial x} \right] - m_{pz} \frac{\partial^2 u(x,t)}{\partial t^2} = F(t) \tag{3.67}$$

where Y_{ij} is the Young's modulus of the piezoelectric material, i is the direction of electric field, j is the direction of mechanical strain or stress, A_p is the cross section and m_p is the mass per unit length of the piezoelectric material. Boundary conditions are defined as:

$$u(x,t) = 0 \qquad \text{at x=0} \tag{3.68}$$

$$Y_{ij} A_{pz}(x) \frac{\partial u(x,t)}{\partial x} = 0 \qquad \text{at x=} h_{pz} \tag{3.69}$$

As mentioned in longitudinal vibration part, the differential equation can be solved for mode shape function by the method of separation variables.

$$u(x,t) = \sum_{r=1}^{\infty} U_r(x)\eta_r(t) \tag{3.70}$$

$$\frac{d}{dx}\left[Y_{ij} A_{pz}(x) \frac{dU(x)}{dx} \right] - w^2 m_{pz}(x) U(x) = 0 \tag{3.71}$$

$$\beta_r = w_r \sqrt{\frac{m_{pz}}{Y_{ij} A_{pz}}} \quad \text{where r=1...}\infty \tag{3.72}$$

$$\frac{d^2U(x)}{dx^2} - \beta^2 U(x) = 0 \tag{3.73}$$

With the application of boundary conditions given in Equations (3.68) and(3.69), Equation (3.73) could be solved and β_r and the mode shape function become

$$\beta_r = (2r-1)\frac{\pi}{2h_{pz}} \quad \text{r=1,2,....} \tag{3.74}$$

$$U_r(x) = A_r \sin(\beta_r x) \tag{3.75}$$

Using orthogonality relations given in Equation(3.76)

$$\int_0^{h_{pz}} U_r(\mathrm{x}) m_{pz} U_s(x) = \delta_{rs} \qquad r,s = 1,2,... \tag{3.76}$$

A_r can be obtained as

$$A_r = \sqrt{\frac{2}{m_{pz} h_{pz}}} \tag{3.77}$$

Mass normalized mode shape function can be defined as

$$U_r(x) = \sqrt{\frac{2}{m_{pz} h_{pz}}} \sin\left[(2r-1)\frac{\pi}{2h_{pz}}x\right] \quad \text{r=1,2,...} \tag{3.78}$$

To find time dependent generalized coordinates, Equation(3.78) is substituted into equation of motion Equation(3.70) and after following same procedure in longitudinal vibration solution undamped modal response η_r becomes:

$$\eta_r(t) = \frac{1}{w_r}\int_0^t F(\tau)\sin w_r(t-\tau)d\tau \quad \text{r=1,2,...} \tag{3.79}$$

$F(t)$ is the total force coming from each layer and is expressed as follows

$$F(t) = F_{pz}U_r(L) + \ddot{b}(t)m_{pz}\int_0^{h_{pz}} U_r(x)dx \quad \text{r=1,2,...} \tag{3.80}$$

Response can be obtaining by substituting Equation (3.78) and (3.79) into Equation (3.70)

$$u(x,t) = \sum_{r=1}^{\infty}\frac{U_r}{w_r}\int_0^t F(\tau)\sin w_r(t-\tau)d\tau \quad \text{r=1,2,...} \tag{3.81}$$

Strain at any point and time in force direction can be calculated as

$$S_j(x,t) = \frac{\partial u(x,t)}{\partial x} \tag{3.82}$$

Stress and force in force direction can also be written

$$T_j = S_j Y_{ij} \tag{3.83}$$

$$F_{pz} = T_j A_{pz} \tag{3.84}$$

3.6.2 Relations with Mechanical and Electrical Parameters of Piezoelectric Stacks

Piezoelectric materials have anisotropic mechanical and electrical properties between its boundaries. Therefore, response or output coming from material changes with respect to polarization and applied force directions. The most general equation could be written to find strain vector (S_j) from stress (T_j) and electric field (E_i) vectors as

$$\begin{bmatrix} S_1 \\ S_2 \\ S_3 \\ S_4 \\ S_5 \\ S_6 \end{bmatrix} = \begin{bmatrix} s_{11}^E & s_{12}^E & s_{13}^E & 0 & 0 & 0 \\ s_{21}^E & s_{22}^E & s_{23}^E & 0 & 0 & 0 \\ s_{31}^E & s_{32}^E & s_{33}^E & 0 & 0 & 0 \\ 0 & 0 & 0 & s_{44}^E & 0 & 0 \\ 0 & 0 & 0 & 0 & s_{55}^E & 0 \\ 0 & 0 & 0 & 0 & 0 & s_{66}^E = 2(s_{11}^E - s_{12}^E) \end{bmatrix} \begin{bmatrix} T_1 \\ T_2 \\ T_3 \\ T_4 \\ T_5 \\ T_6 \end{bmatrix} + \begin{bmatrix} 0 & 0 & d_{31} \\ 0 & 0 & d_{32} \\ 0 & 0 & d_{33} \\ 0 & d_{24} & 0 \\ d_{15} & 0 & 0 \\ 0 & 0 & 0 \end{bmatrix} \begin{bmatrix} E_1 \\ E_2 \\ E_3 \end{bmatrix} \tag{3.85}$$

Using the same methodology, electrical displacement vector (D_i) could be found as

$$\begin{bmatrix} D_1 \\ D_2 \\ D_3 \end{bmatrix} = \begin{bmatrix} 0 & 0 & 0 & 0 & d_{15} & 0 \\ 0 & 0 & 0 & d_{24} & 0 & 0 \\ d_{31} & d_{32} & d_{33} & 0 & 0 & 0 \end{bmatrix} \begin{bmatrix} T_1 \\ T_2 \\ T_3 \\ T_4 \\ T_5 \\ T_6 \end{bmatrix} + \begin{bmatrix} \varepsilon_{11} & 0 & 0 \\ 0 & \varepsilon_{22} & 0 \\ 0 & 0 & \varepsilon_{33} \end{bmatrix} \begin{bmatrix} E_1 \\ E_2 \\ E_3 \end{bmatrix} \tag{3.86}$$

For the single direction force and polarization, the Equations (3.85) and (3.86) could be simplified as

$$S_j = s_{ij}^E T_j + d_{ij} E_i \tag{3.87}$$

$$D_i = d_{ij}^E T_j + \varepsilon_{ij} E_i \tag{3.88}$$

3.6.3 Calculation of Electrical Power Generations in Quasi-Static Loading Conditions

Basic relations are given in the previous part of modelling piezoelectric material and these resulting formulae are used to predict the power generation of the piezoelectric material. As given in the section title, the calculations are given for the quasi-static loading conditions, which mean that the excitation occurs at much lower frequencies than resonance frequencies of piezoelectric material. Natural frequencies of the piezoelectric stacks appear in kHz range, whereas excitation frequencies in beam-like structures are well below. For the compression mode of piezoelectric stacks, solutions are given in quasi-static loading case; on the other hand, beam like piezoelectric materials have lower natural frequencies and they can be used at their resonance frequencies. For the dynamic conditions; i.e., operating at resonance frequencies, Mason model could be used to analyse piezoelectric material. However, in this method equivalent circuitry are very complex and reducing parameters into simple forms require more time when compared to the quasi-static solution form.

Stacks used in this work polarized in the *3*rd direction; in other words, poling is 3rd direction and also force is applied in the *3*rd direction; therefore, the solution used to model piezo and to find the electric outputs is valid for the *33* direction.

The relation between electric field and stress consisted on piezo layer

$$E = g_{33}T \tag{3.89}$$

and g_{ij} represents the piezoelectric voltage constants and gives the linear relation between electric field and stress.

Charge produced in piezo because of the force applied on layer as:

$$Q_{pz} = d_{33}F_{pz} \tag{3.90}$$

and d_{ij} represents piezoelectric charge constant.

Charge could be described also by using electrical relations between electrical displacement and electric field

$$Q_{pz} = DA_{pz} \tag{3.91}$$

$$D = E\varepsilon_0\varepsilon_{3,r}^{T} \tag{3.92}$$

ε_0 is the permittivity of the free space and $\varepsilon^{T}_{3,r}$ is the permittivity of the piezoelectric material for constant stress conditions.

From equilibrium of Equation (3.90) and (3.91), the relation Equation (3.93) between piezoelectric material properties could be obtained.

$$d_{33} = g_{33}\varepsilon_0\varepsilon_{3,r}^{T} \tag{3.93}$$

The equivalent voltage produced in piezo layer against charge could be found

$$V_{pz} = \frac{Q_{pz}}{C_{pz}} \tag{3.94}$$

Capacitance is also defined as

$$C_{pz} = \frac{\varepsilon_0 \varepsilon_{3,r}^T A_{pz} A_f}{h_{pz}} \tag{3.95}$$

where h_{pz} is the height of the piezoelectric material and A_f is the area fraction of the electrodes surface to the area of whole layer and should be obtained from the producer of the piezoelectric material.

Piezoelectric stacks consisting of '*n*' layers can be designated as capacitance elements connected in parallel as shown in Figure 28.

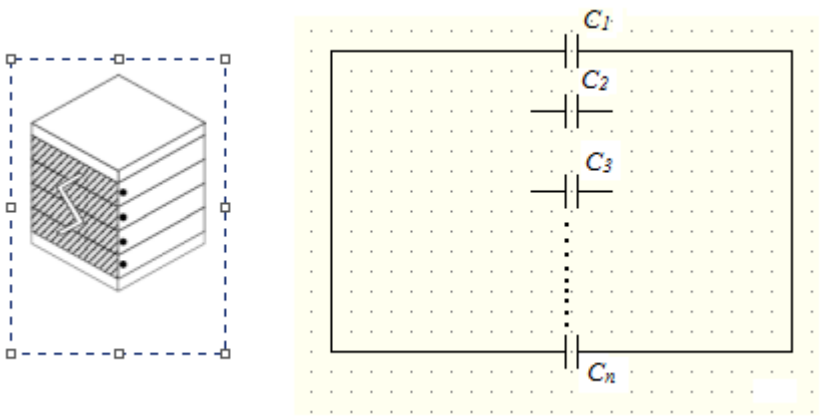

Figure 28: Sample Showing the Electrical Connection of Piezoelectric Stacks

Therefore, the relations given for piezo could be updated for stack

$$Q_s = nQ_{pz} \tag{3.96}$$

$$C_s = nC_{pz} \tag{3.97}$$

In other words, charge capacity of a multilayer piezoelectric material is larger than a single layer material with the same height of total layers. Table 1 describes these relations in detail.

Table 1: Relations between Multilayer and Single Layer Piezoelectric Materials Having Same Height [9]

Type of Piezoelectric Material	**Capacitance**	**Produced Charge**	**Produced Voltage (Open Circuit)**	**Harvested Energy**
Single Layer Piezoelectric Material	$C_{pz} = \frac{\varepsilon_0 \varepsilon_{3,r}^T A_{pz} A_f}{h_{pz}}$	$Q_{pz} = Q$	$V_{pz} = V$	$W_E = \frac{1}{2}\frac{Q_{pz}^2}{C_{pz}}$
Multilayer Piezoelectric Material	$C_s = n\frac{\varepsilon_0 \varepsilon_{3,r}^T A_{pz} A_f}{h_{pz}/n}$	$Q_s = nQ = nQ_{pz}$	$V_s = \frac{V}{n} = \frac{V_{pz}}{n}$	$W_E = \frac{1}{2}\frac{Q_s^2}{C_s} = \frac{1}{2}\frac{Q_{pz}^2}{C_{pz}}$

For the piezoelectric material, harvested electrical energy could be written as

$$W_E = \frac{1}{2}\frac{Q_s^2}{C_s} = \frac{1}{2}C_s V_s^2 \tag{3.98}$$

Transmitted mechanical energy into the piezoelectric material is also described as

$$W_M = F_{pz} x_{pz} \tag{3.99}$$

The ratio of the harvested energy to the transmitted energy gives the electromechanical coupling coefficient k_{33}

$$k_{33} = \frac{W_E}{W_M} \tag{3.100}$$

This property gives the simple result for the efficiency of the harvesting process.

During the harvesting process some losses occur in stacks and they should be included in the governing equation.

Figure 29 shows the equivalent circuit design for piezoelectric material under quasi-static working conditions. There are two resistances inserted into the circuit, namely R_{loss} and $R_{leakage}$. R_{loss} is the loss coming from current travelling through the surfaces of piezoelectric material and can be calculated using loss tangent property of the material and operating frequency.

$$R_{loss} = \frac{\tan(\delta)}{C_s w} \tag{3.101}$$

$R_{leakage}$ is the loss coming from current travelling through the material. The value of this loss should be measured. Detailed explanation about this measurement is given in the following chapter.

Figure 29: Equivalent Circuit Design for Piezoelectric Stack

3.7 Case Study: Responses of Impacting Beam by Analytic Methods

In order to demonstrate the outputs that could be obtained from analytical solution procedure, a case study is performed. The material properties of beam and stopper used in this procedure are given in Table 2.

Table 2: Material Properties of the Beam and the Stopper

	Cantilever Beam (Aluminum,7075)	**Stopper (Stell,11SMnPb30)**
Young Modulus (GPa)	73	190
Density(kg/m^3)	2700	7850
Length(mm)	100	10
Width(mm)	13	20
Thickness(mm)	2	1

The tip mass consists of piezoelectric material, steel piece and the holding screw which is used to hold both materials and to attach them onto the top

surface on cantilever beam. Total mass of the tip mass system is 11×10^{-3} kg and mass moment of inertia about bending axis is calculated to be 6.2713×10^{-3} kg.m^2.

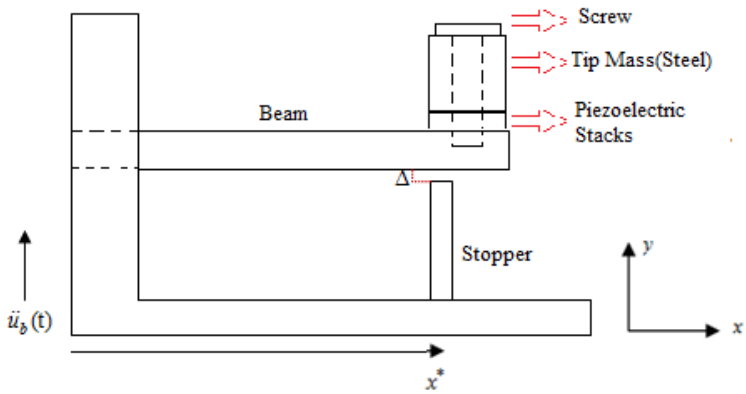

Figure 30. The Schematic Drawing of System used in Analytical Modelling

All the solution procedure is performed in MATLAB R2013b. As mentioned in the analytical procedure part, the time step is the most important parameter in the solution of the equations and it should be at least twice times the period corresponding to the highest natural frequency considered to calculate response of the cantilever beam to avoid aliasing problems. Base excitation is specified as 2.3 m/s^2 at a frequency of 63.2 Hz which is equal the first natural frequency of the beam. The response of cantilever beam without impact conditions is shown in Figure 31. The methodology to find damping ratios is given in experimental section.

As the base excitation is taken equal to the first natural frequency of the cantilever beam, only the harmonic response at the first natural frequency is seen in the figure. For the response calculation, the first 5 modes are used in

the solution and convergence study is performed for the case when impact is included in the motion. Beam makes the motion 7.3×10^{-4} m band, therefore; stopper is placed at $3*10^{-4}$ m below of the beam and its motion is given in Figure 32. Stopper response is very low when compared to the beam as the base excitation frequency is far away from the first natural frequency of the stopper.

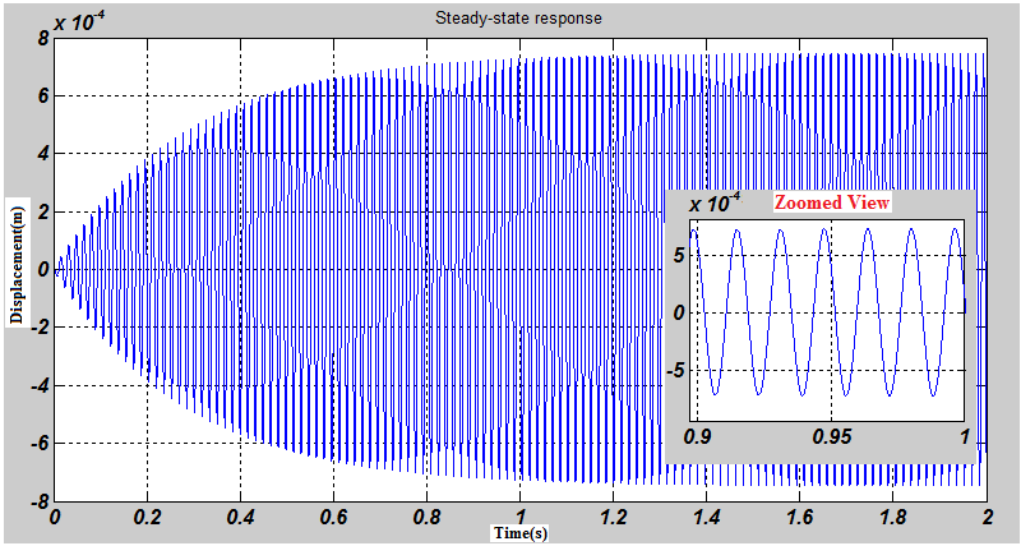

Figure 31: Steady-State Response of a Cantilever Beam under Base Excitation, f=63.2Hz

The beam and stopper move together when the impact occurred. Therefore, in each time step, whether they move together or not should be viewed. Figure 33 shows the motion of the beam in impact and without impact conditions. When the impact occurs, the displacements of beam and stopper are equalised.

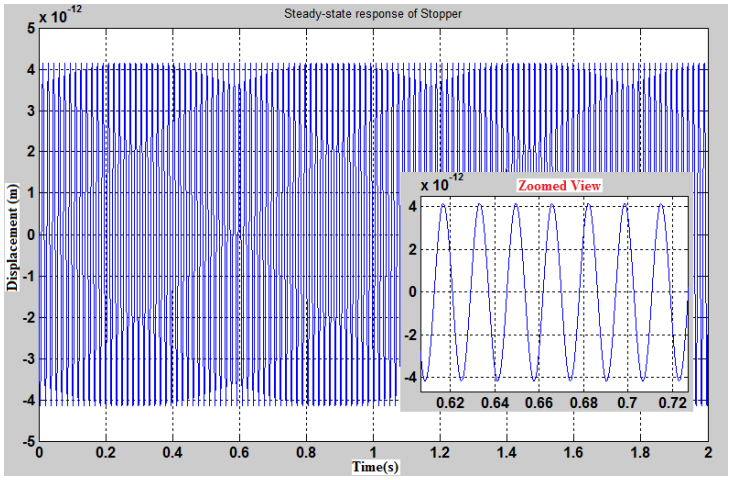

Figure 32. Steady-State Response of the Stopper under Base Excitation, f=63.2 Hz

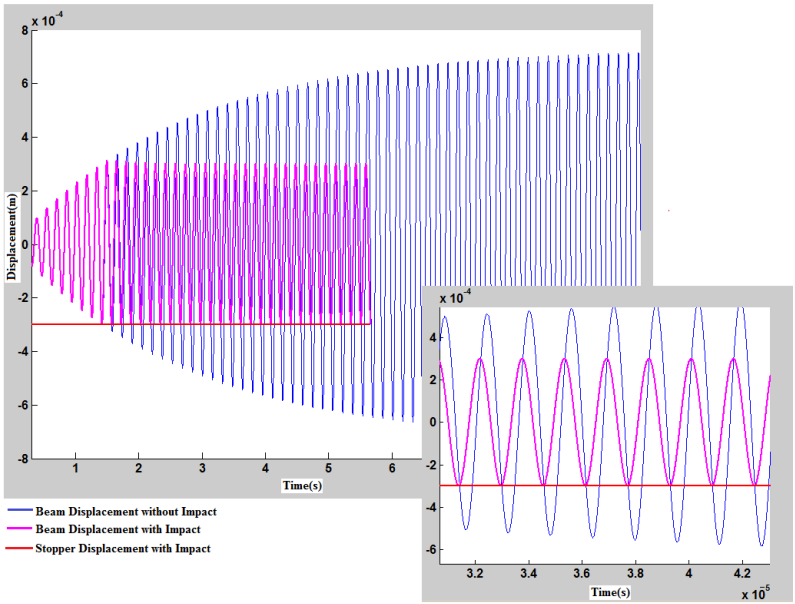

Figure 33. Steady-State Responses of Beam and Stopper with and without Impact Conditions

Figure 34 shows the detailed view of impact duration. Depending on the time step used in solution, smoothness of the impact duration is increased. In other words, pink (beam) and red(stopper) lines move together. However, short time

steps imply longer solution times. Therefore, convergence studies should be performed to find which time step is more efficient and gives the accurate results. In this work, time step is taken 10^{-6} which is ten times the period corresponding to the highest natural frequency of interest.

Figure 35 shows the results of choosing large time step. In this case, either impact duration could not be caught or responses start to diverge. This is because; there is a considerable difference between responses of beam and stopper at the time of impact. As mentioned in the solution of impacting beam problem, analytical force calculation is an iterative procedure. Before the time of impact, the displacement of the beam comes from base excitation. However, after impact, total response is summation of the base excitation and impulse response due to impact. When the numerical solution senses the time of impact, the beam position could be lower than the stopper. At that instant, a calculated force value is inserted in the impulse response function. If the difference between positions is relatively high, calculated force becomes very large and as a result of this large impact force the response of the beam diverges.

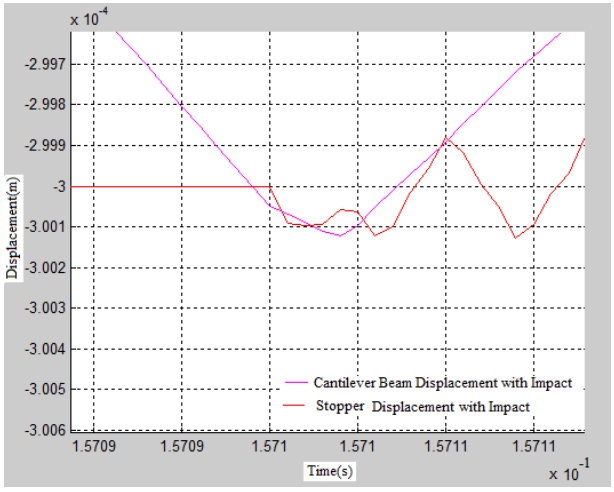

Figure 34. Zoomed View of Impact Moments

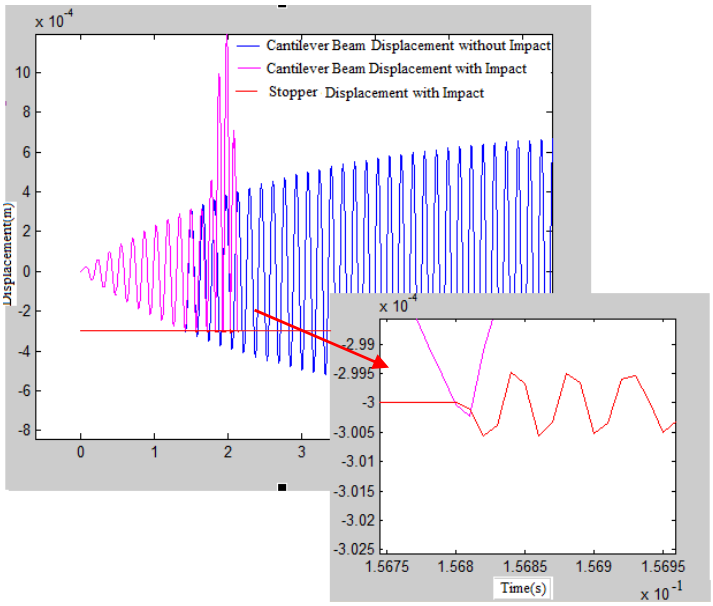

Figure 35. Responses for the Large Time Step

As the beam does not always move with the stopper during the motion, chattering occurs between two bodies. The motion of the beam is limited by the stopper and therefore, the impact force occurs between them. The impact force reacts against the beam repeatedly. The resulting force development can be seen in Figure 36.

The velocity and acceleration changes during the impact could be seen in Figure 37. Up to the time of impact, because of the base excitation, only first natural frequency oscillations dominate the motion. However; after the impact takes place, the modes at high frequencies also arise. Therefore, small oscillations in basic form of velocity and acceleration involving impacts can be seen.

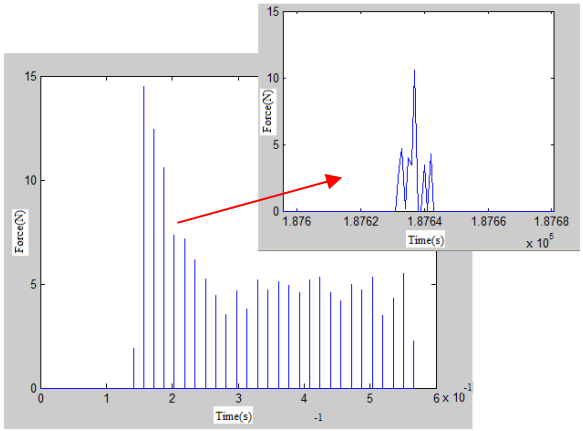

Figure 36. Contact Force Obtained Impact Moment

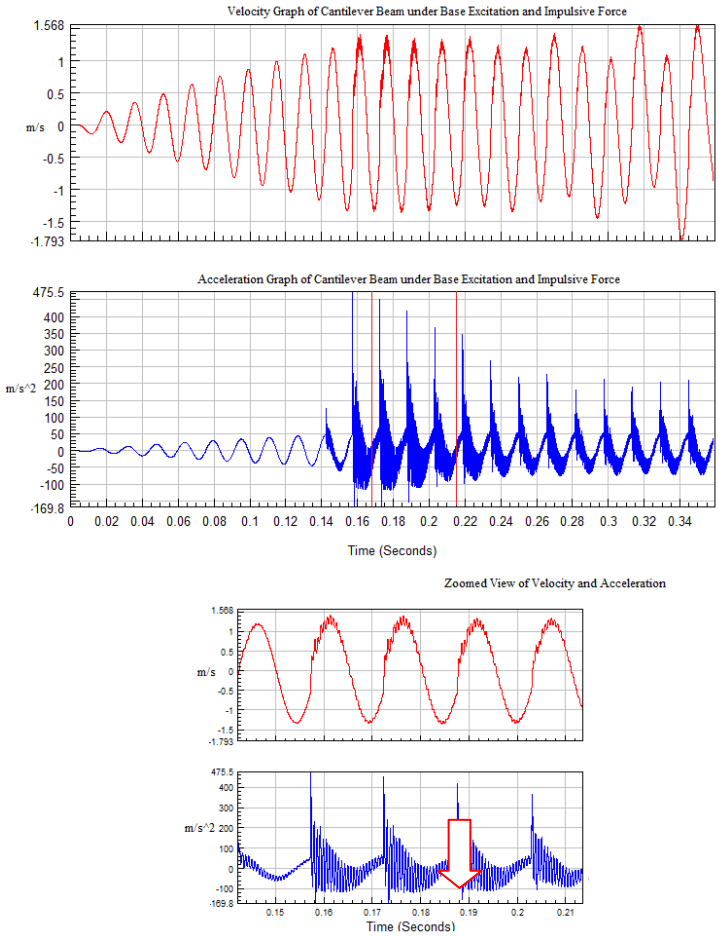

Figure 37. Velocity and Acceleration Histories of Cantilever Beam under Base Excitation and Impulsive Force

Figure 38 shows the voltage production of piezoelectric material with and without impact conditions, obtained by the analytical expression given in modelling of piezoelectric stacks part. Distributed and lumped parameter solutions are compared during the solution of impact case, Red line in Figure 38 represents the case when mass of each layer is included in the solution. Results shown with the blue line stands for the case where piezoelectric material is thought as a bulk material and calculations are carried by taking total mass of the piezoelectric material. Green line refers to the voltage production without impact condition.

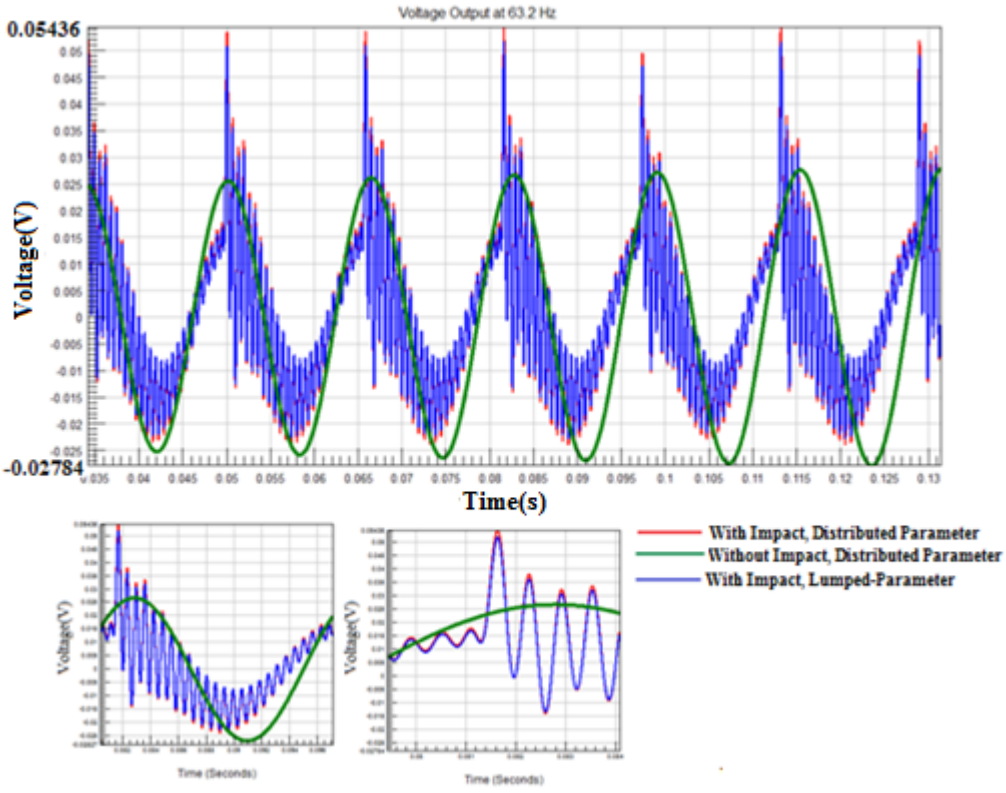

Figure 38. Voltage Production under Base Excitation, with Impact and without Impact Condition

In experimental measurement of the voltage output, some losses occur due to internal resistances and capacitance of the piezoelectric material as mentioned in the early part of the chapter. Therefore, voltage output given in Figure 38 should be modified using equivalent circuit of measurement case. Leakage resistance and capacitance measurements are performed in experimental section and values are found as 14.1 mega-ohms and 385nF. Loss resistance depends the excitation frequency and for the case where excitation frequency is 63.2 Hz it is calculated as 111.2 ohm by Equation(3.102). Figure 39 and Figure 40 show the equivalent circuit and voltage comparison after including leakage and loss resistance.

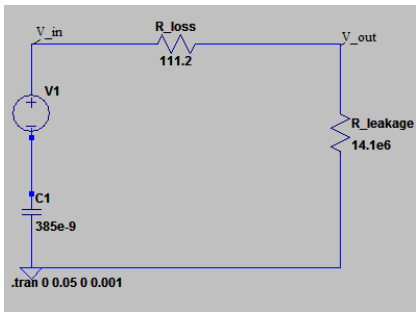

Figure 39. Equivalent Circuit Design for Analytical Voltage Output

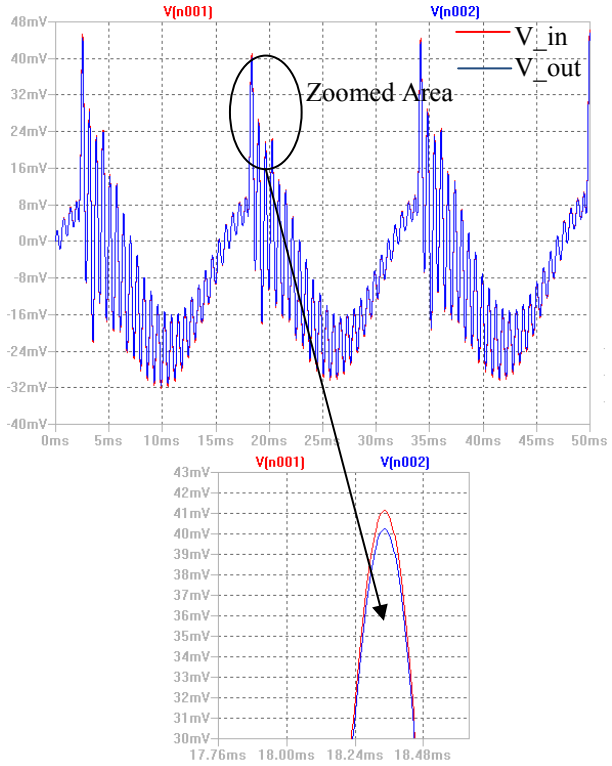

Figure 40. Comparison of Produced Voltage before Losses and After Losses

CHAPTER 4

EXPERIMENTAL STUDIES

In this part of the study, results of experiments and their comparison with their analytical counterparts are discussed and evaluated comparatively. The chapter starts with validation of analytical solutions in reference to experimental results. Later in the chapter, frequency dependence of harvester voltage output is investigated. In the last part, effects of stopper bar location on the harvester efficiency are discussed.

In the experiments CMAR03 piezoelectric stacks are employed to measure voltage output. Piezoelectric stacks have 25 layers made up of NCE57ceramics. The picture can be seen in Figure 41. Isolation material is used between the beam and the piezoelectric material layers as well as under the compression mass resting on the top of piezoelectric layers during the mounting process.

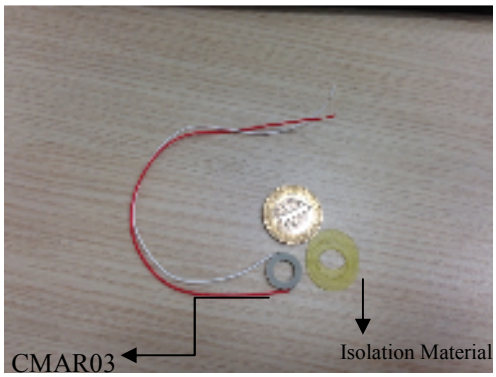

Figure 41. CMAR03 Piezoelectric Material produced by Noliac Company

Experiment test setup used in this work is similar to Mak *et al*. [26], however; the latter study employs a piezoelectric beam as opposed to the piezoelectric stack in this study. Also, during the continuous modelling process, strain equations are not included the response of cantilever beam because of difference in piezoelectric material configuration in both harvesters. The harvester signed and built in this study is shown in Figure 42. In this case, the stopper is used to investigate effects of impacts on energy harvesting. The test setup shown in Figure 43 is intended to identify dynamic characteristics of the cantilever beam with base excitation and tip mass. Piezoelectric material and tip mass on the beam is screwed to the beam and the accelerometer is glued on the mounting screw as shown.

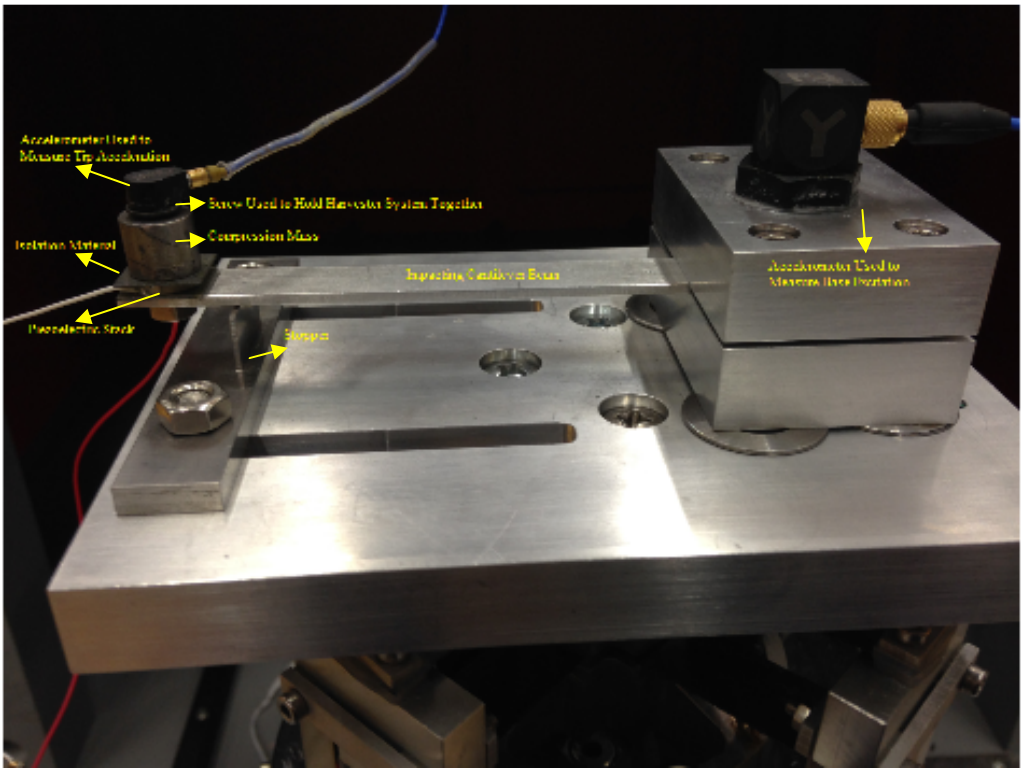

Figure 42. Experimental Setup Used for Impacting Beam

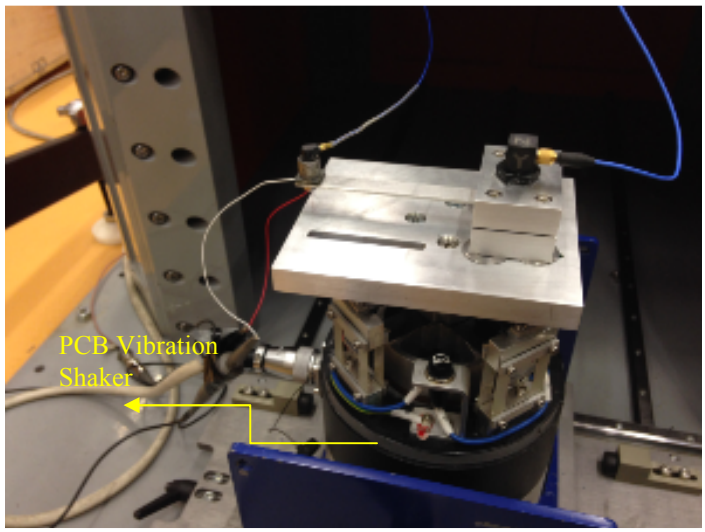

Figure 43. Experimental Setup Used for not Impacting Case

4.1 Damping Correction for the Analytical Model

Steady-state response can be found by a distributed parameter model of the harvester as mentioned in the previous chapter. However, damping ratio depends on dynamic properties of the system and there exist different experimental ways of finding these ratios. In analytical solution part, it is assumed that the response of the beam is composed of only responses at natural frequencies of the beam. The validation of this assumption is performed in the following section and discussions are also given in conclusion chapter. Therefore, to find damping a ratio, harmonic motion is applied at its base to the harvester at natural frequencies of the beam. As shown in Figure 43, acceleration levels from the base and tip mass location are measured. Damping ratios could be found by inserting measured acceleration levels in Equation (4.1). For this study, damping ratios for first four natural frequencies are found as shown in Table 3.

The response of the beam could also be found as,

$$X(iw) = \frac{1 + i2\zeta w / \mathrm{w}_n}{1 - (w / \mathrm{w}_n)^2 + i2\zeta w / \mathrm{w}_n} Y \quad \text{where } Y \text{ is the base excitation amplitude} \tag{4.1}$$

Table 3. Damping Ratios of Cantilever Beam

Mode 1	63.2 Hz	0.0093
Mode 2	615.32 Hz	0.162
Mode 3	1566.7 Hz	0.015
Mode 4	3193.1 Hz	0.09
Mode 5	5927.9 Hz	0.09

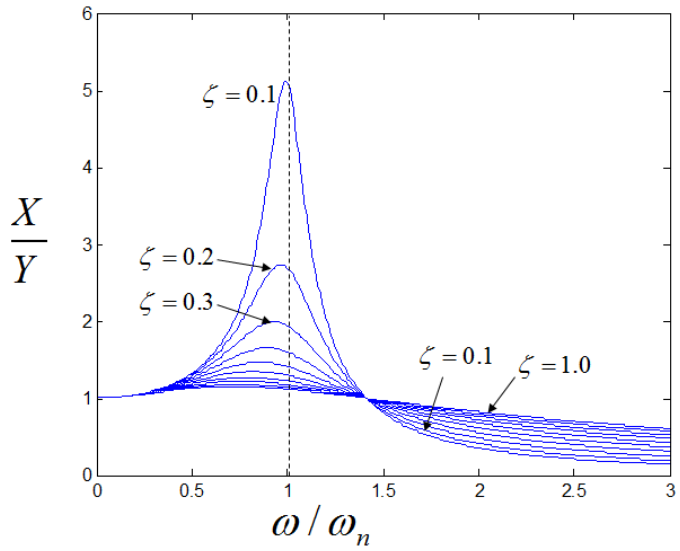

Figure 44. Effects of Damping on Response Amplitude [34]

In experiments, PCB 2100E11 model shaker is used and its frequency band is up to 4 kHz. Therefore, for the 5^{th} natural frequency, 4^{th} mode damping ratio is taken.

4.2 Experimental Validation of Analytical Solutions for Impacting Beam

In theorical part of the study, numerical results obtained from analytical solution are shared. In this part, their validation with experiments is discussed and the graphical results are given in the following part of this section.

Some differences between experimental results and analytical solutions could be seen. However, in analytical modelling, mode expansion theorem is used with responses to both harmonic base excitation and impulsive excitation at the location of the stopper. Therefore, in analytical solution, effects of only first 5 natural frequencies are seen. Though, in experimental response, contributions at all frequencies take part in the total response.

In analytical solution, impact forces are obtained and used in response calculation. However; in experimental study, response of the beam is measured by an accelerometer. Therefore, impact forces could not be obtained in experiments due to insufficiency of instrumentation for impact forces developed. Load cell could have been employed to measure the impact force, yet; stopper characteristics change, therefore; its corresponding continuous model should have been prepared [30]. However, this alternative is not exercised due to complexity of modelling the load cell and uncertainties it could introduce.

In experiments, first natural frequency of the cantilever beam is observed as 62.5 Hz which is almost the same with theoretical case. The experimental burst random test result is shared in Figure 45. The measurements are performed by LMS Test Lab software and PCB 356A16 and 352A24 accelerometers.

Accelerometers are glued on the clamped end of the beam and tip mass using Loctite 401. Frequency resolution is 0.25 Hz and a sampling frequency 2048 Hz is assigned. Number of averages in spectral analysis is 40. Block size is 8192.

The validation between two methods is performed for tip displacement, acceleration and voltage output with and without impact cases. These responses are shown in Figure 46 – 48. Time response measurement is performed using Dewesoft software and Dewetron data acquisition system (DEWE 510) due to its capability of acquiring continuous time data.

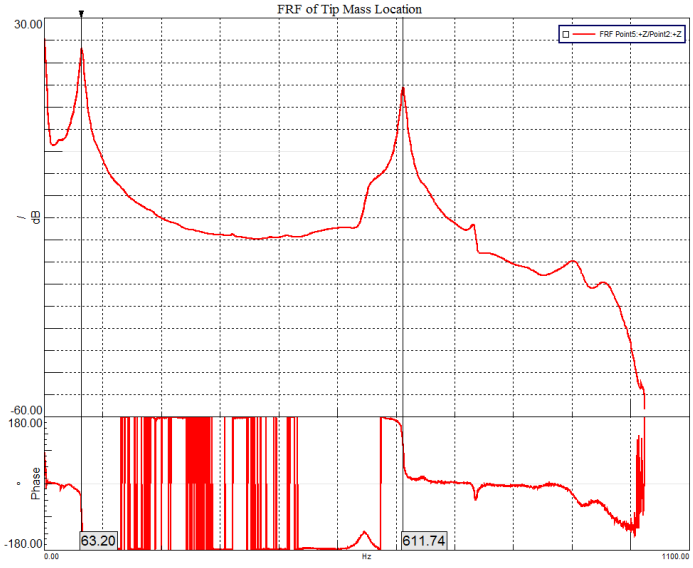

Figure 45. Experimental Frequency Response Function of Tip Mass Location

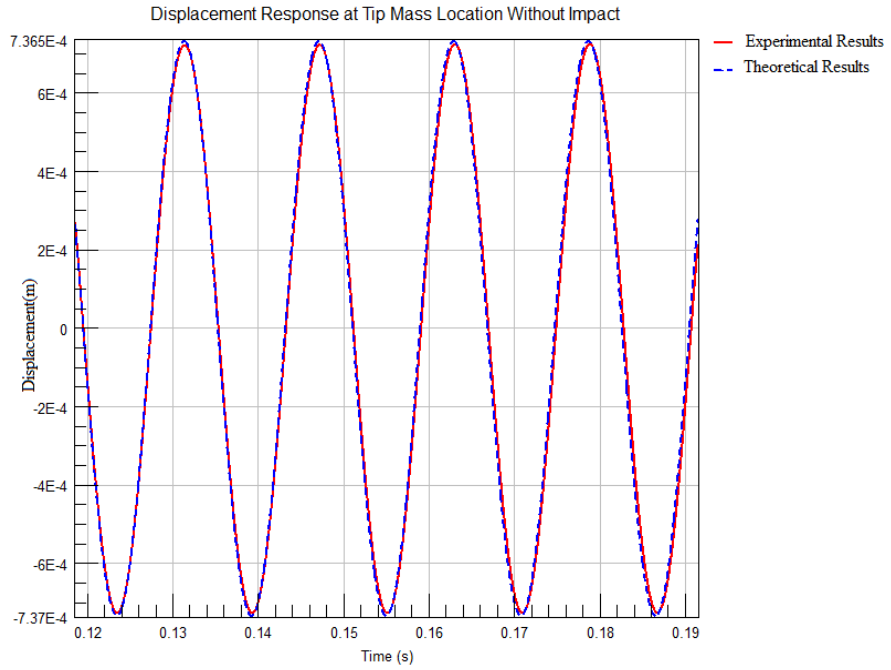

Figure 46. Steady-State Displacements of Tip Mass Location without Impact Conditions

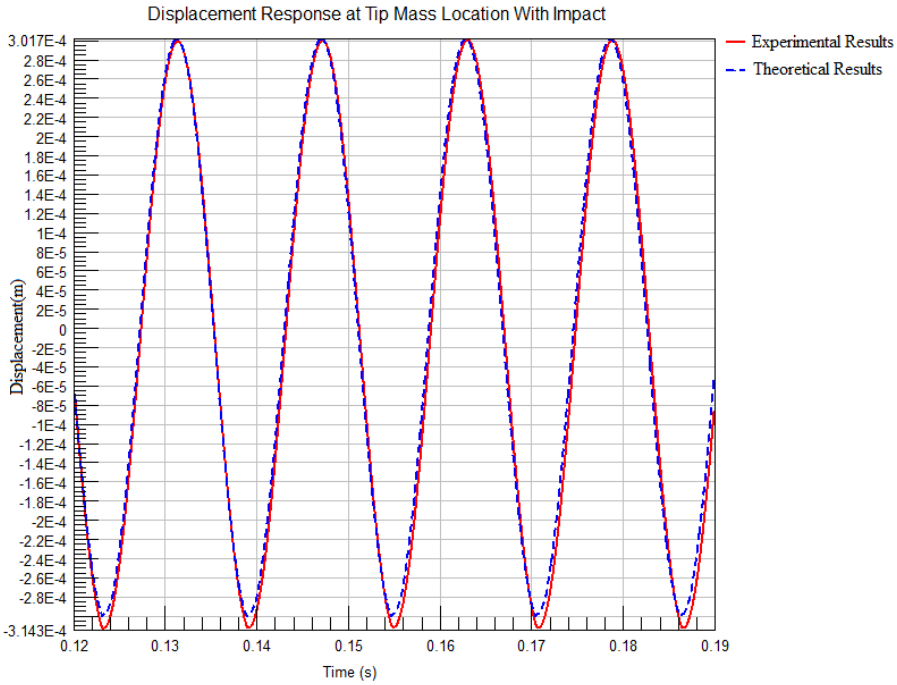

Figure 47. Steady-State Displacements of Tip Mass Location with Impact Conditions

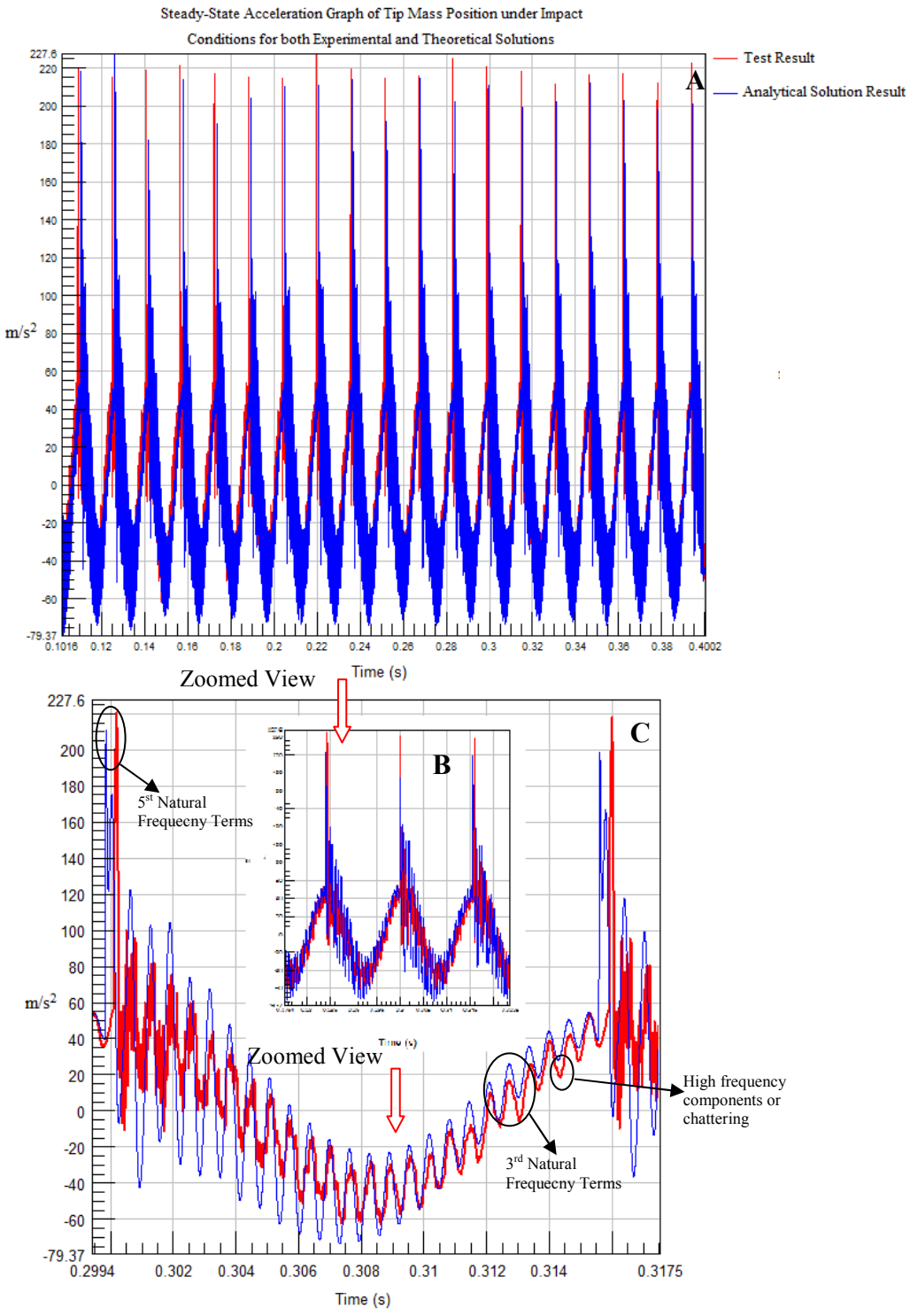

Figure 48. Steady-State Acceleration History of Tip Mass Position under Impact Conditions for both Experimental and Theoretical Solutions, A-Total Response, B- Zoomed View of A, C- Shows One Oscillation at 62.5Hz

Displacements with and without impact conditions are almost same when experimental and theoretical results are analysed. Their oscillation frequencies are observed as 62.5 Hz(experimental) and 63 Hz(theoretical), respectively. In acceleration time histories, it is discovered that base or first natural frequency motion still keeps the main harmonic form, as the base excitation comes to the beam is the same as with that of due to the first natural frequency of the cantilever beam. However, during this motion high frequency terms are also included in acceleration because, impact force excites the higher natural frequencies as well. The zoomed view given in Figure 48-C shows one oscillation at 62.5 Hz. Small oscillations at the first part of the motion comes from 5th natural frequency of the beam at 5962 Hz and the other oscillation within the cycle is associated with the 3rd natural frequency at 1612Hz. Moreover, in the experiments involving impacts, high frequency components or chattering are observed on the whole response. High frequency components are expected in the response since impacts generate sub and super harmonics of the excitation frequency due to its nonlinear nature. Effects are found to be present in zoomed acceleration time histories. Figure 49 shows the rms power spectrum of tip acceleration in impacting process up to 3 kHz. Inserting a stopper to the system converts linear system to a nonlinear one, introducing a backlash effect. This non-linear terms cause harmonics of excitation within a frequency bandwidth. A more detailed work to understand this non-linear effect is performed in the following section.

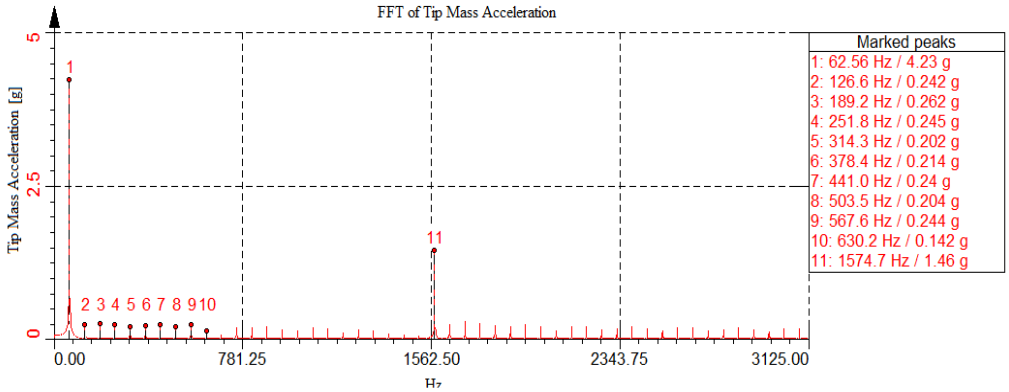

Figure 49. Experimental rms Power Spectrum of Impacting Cantilever Condition

4.3 Harmonic Base Acceleration Experiments at Different Frequencies with Impact and without Impact Conditions

Small deviations in the input excitation frequency from any natural frequency are expected to cause excessive decrease in the power output. Therefore, increasing the frequency bandwidth of the harvester enables the harvester to be used in broadband loading environments. For this reason, in this part of the work, harmonic motions of differing frequency are introduced as input by using PCB 2100 E 11 shaker to understand the effects of stopper on the effective frequency bandwidth of the harvester.

Experience with the accelerometers in the tests has disclosed insufficiency of amplitude range. Natural frequency of the beam is decreased to 56.2Hz by increasing the tip mass to extend the working frequency bandwidth. At higher frequency excitations such as 90Hz, the accelerometer located on the tip mass location is found to be saturated. Hence, drop in natural frequency equips the harvester with a wider band of operation. For this purpose, white noise shown in Figure 50 is given as an input to realize effects of impact on frequency response functions of the harvester.

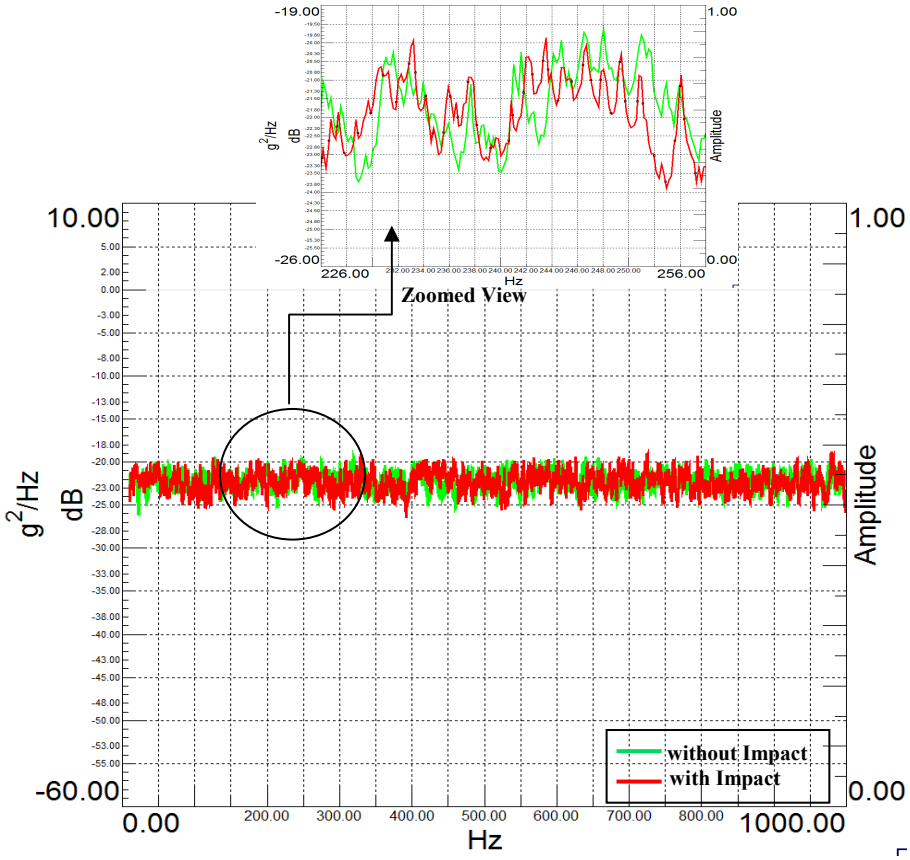

Figure 50. Power Spectral Density (PSD) of Input White Noise to the Harvester

For the control of shaker and measurement of acceleration levels, LMS Test Lab data acquisition system is used. In the measurements, frequency resolution is specified as 0.195313 Hz, maximum frequency of interest is 1000 Hz, sampling frequency is 3200 Hz and number of averages is 40. The frequency response characteristic is obtained by the closed looped controlled white noise given in Figure 50 is shown in Figure 51. Between 35 Hz and 58 Hz, amplitudes in non-impacting conditions are found to be larger than those of impacting conditions. In this particular case, this range of frequencies are very close the cantilever natural frequency which is 56.2 Hz. However, during the

impact, natural frequency shifts to the right of 56.2 Hz and cover a wider range such as from 55 Hz to 66 Hz.

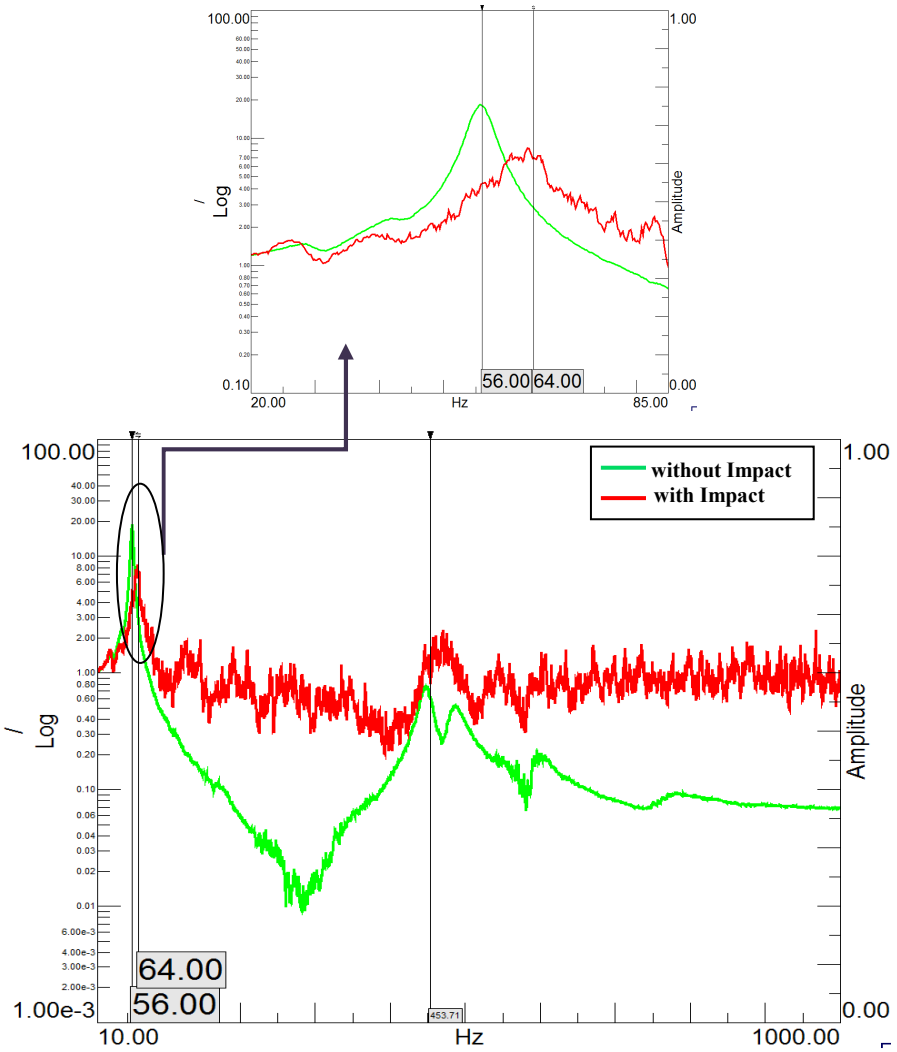

Figure 51. Frequency Response Characteristic Graph of Tip Mass Location

In the white noise experiment, voltage measurement is also performed in both impact and no impact conditions. Figure 52 shows the voltage production in

piezoelectric material in each case. When the time history of the voltage produced is investigated, measured voltage levels are discovered to be very high compared to the non-impacting conditions. These indicate the impact with stopper and excitation of the wider frequency band.

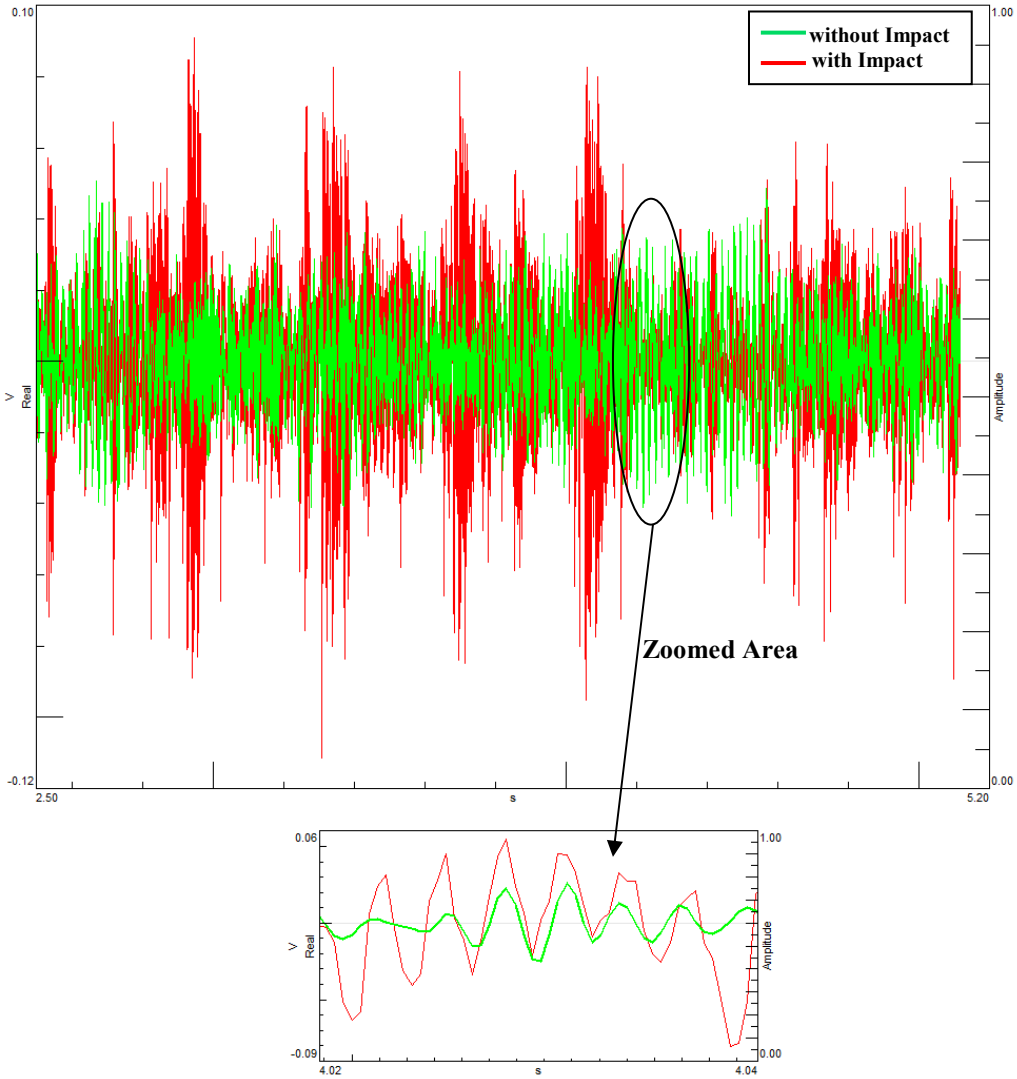

Figure 52. Voltage Measurement in White Noise Experiment

Impacts lead to decrease in amplitude of response at natural frequency. On the other hand, natural frequency band expands to the right of natural frequency and this yields an increase in other frequency response outputs as shown in Figure 51. Therefore, to validate these extractions, cantilever beam is vibrated with difference frequencies both with impact and without impact conditions for the same base excitation levels. Compared frequencies during the harmonic loading are 30, 40, 45, 50, 56, 60, 65, 70, 75 and 80 Hz. For these frequencies, voltage output time histories are presented in Figure 53 to Figure 62. For the time history measurement of voltages, Dewesoft software is used and sample frequency is taken as 100 kHz. A fourth order, analogue low pass filter with a cut off frequency of 20 kHz is also used in the measurement. The gap size between stopper and beam is measured as 3×10^{-4} m by control jig.

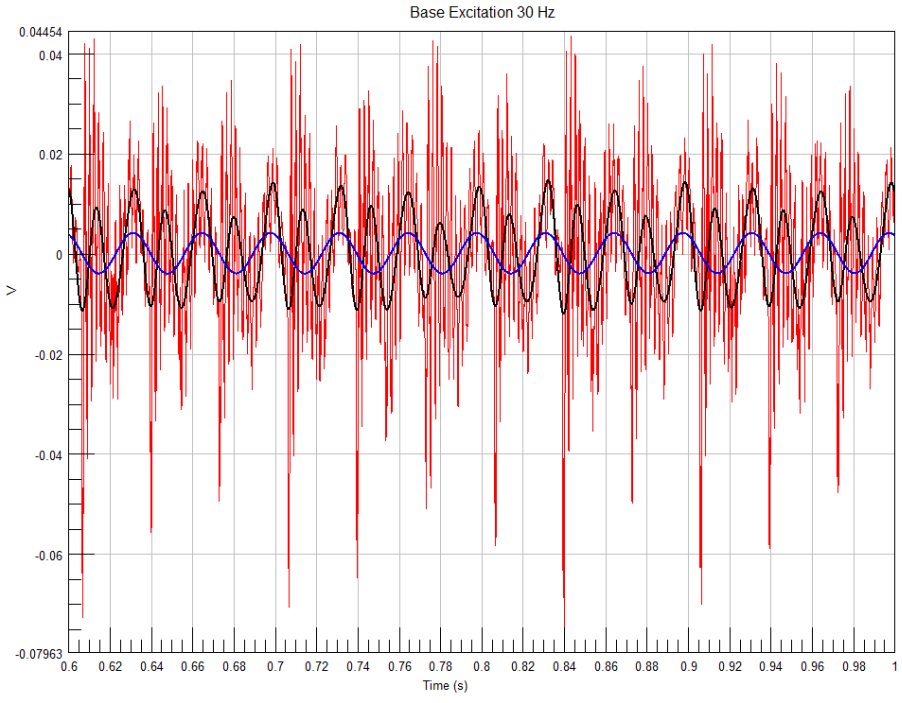

Figure 53. Piezoelectric Material Voltage Outputs at 30 Hz; Blue: without impact, Red: with impact, Black: with impact and 100 Hz low-pass filtered.

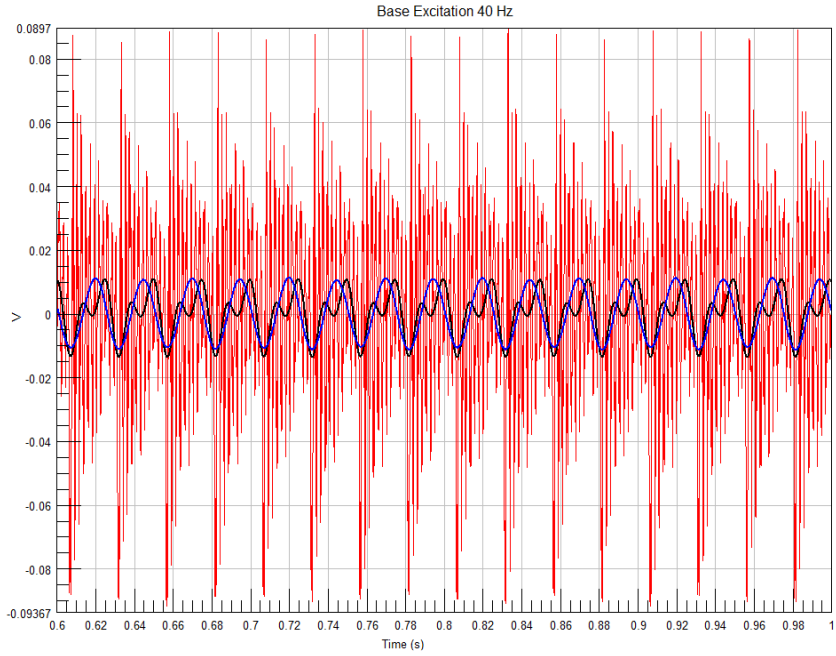

Figure 54. Piezoelectric Material Voltage Outputs at 40 Hz; Blue: without impact, Red: with impact, Black: with impact and 100 Hz low-pass filtered.

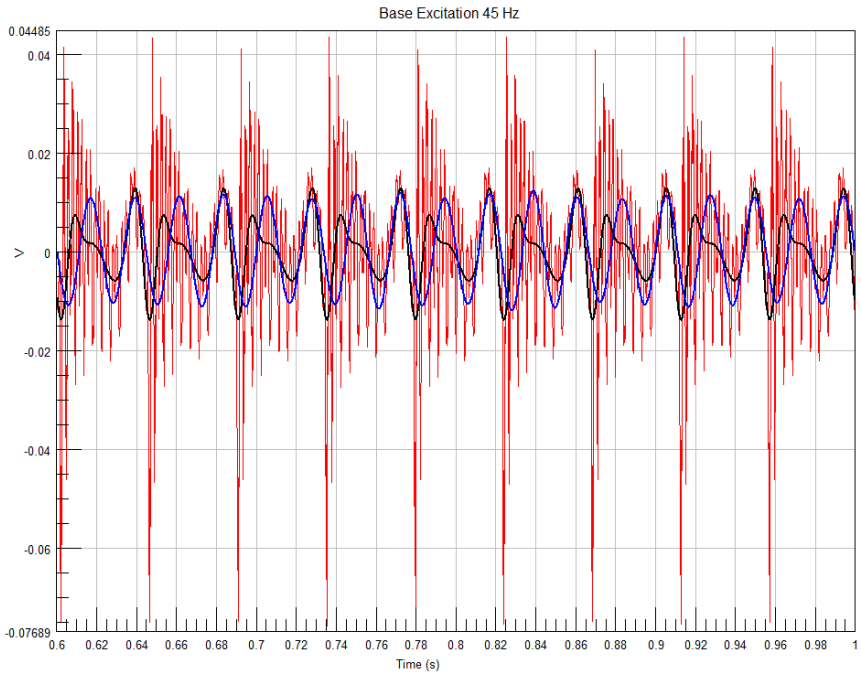

Figure 55. Piezoelectric Material Voltage Outputs at 45 Hz; Blue: without impact, Red: with impact, Black: with impact and 100 Hz low pass-filtered.

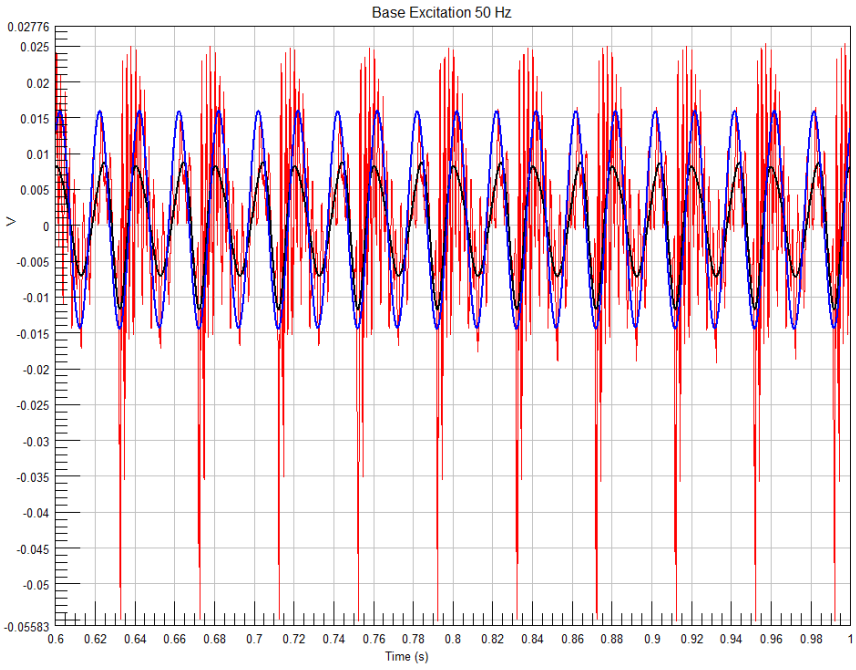

Figure 56. Piezoelectric Material Voltage Outputs at 50 Hz; Blue: without impact, Red: with impact, Black: with impact and 100 Hz low pass-filtered.

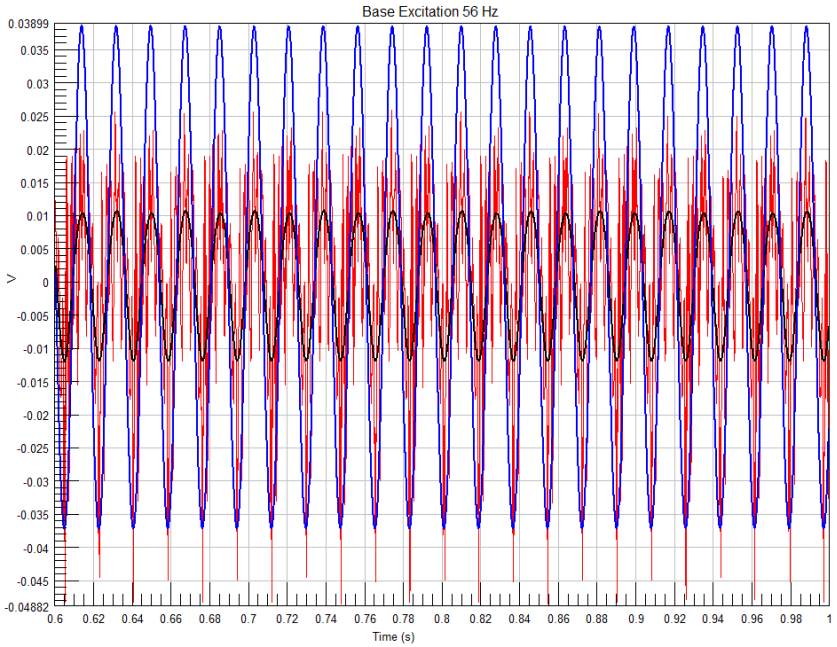

Figure 57. Piezoelectric Material Voltage Outputs at 56 Hz; Blue: without impact, Red: with impact, Black: with impact and 100 Hz low pass-filtered.

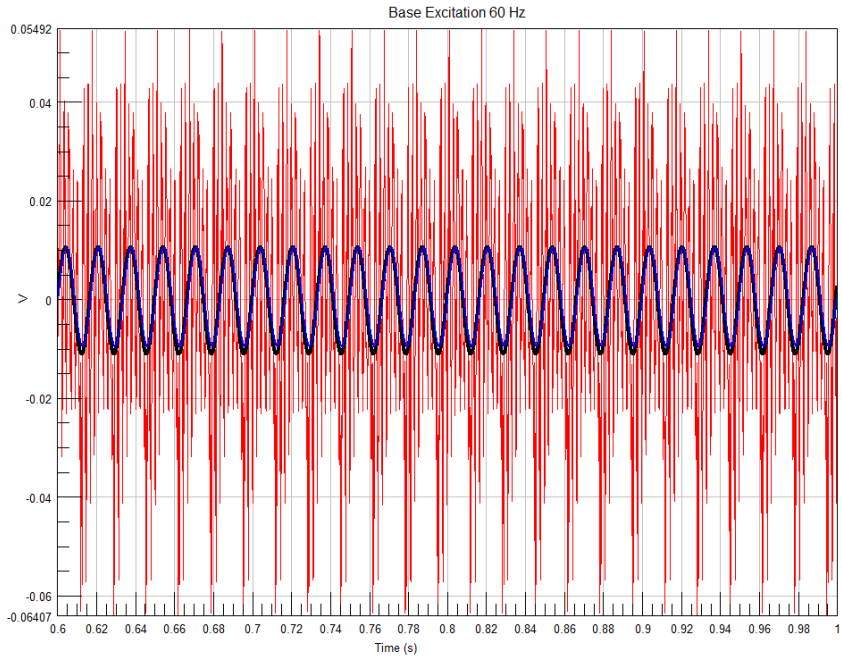

Figure 58. Piezoelectric Material Voltage Outputs at 60 Hz; Blue: without impact, Red: with impact, Black: with impact and 100 Hz low pass-filtered.

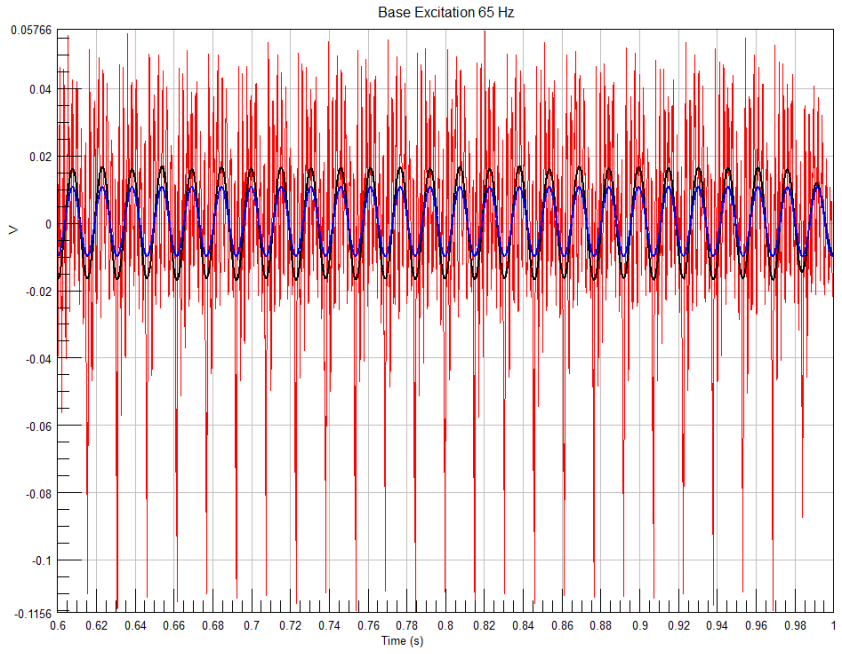

Figure 59. Piezoelectric Material Voltage Outputs at 65 Hz; Blue: without impact, Red: with impact, Black: with impact and 100 Hz low pass-filtered.

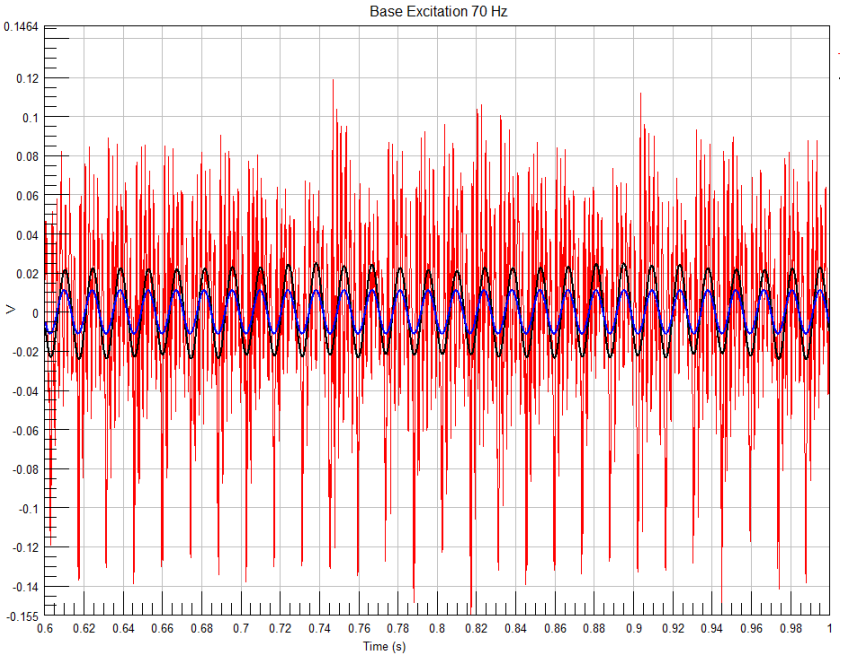

Figure 60. Piezoelectric Material Voltage Outputs at 70 Hz; Blue: without impact, Red: with impact, Black: with impact and 100 Hz low pass-filtered.

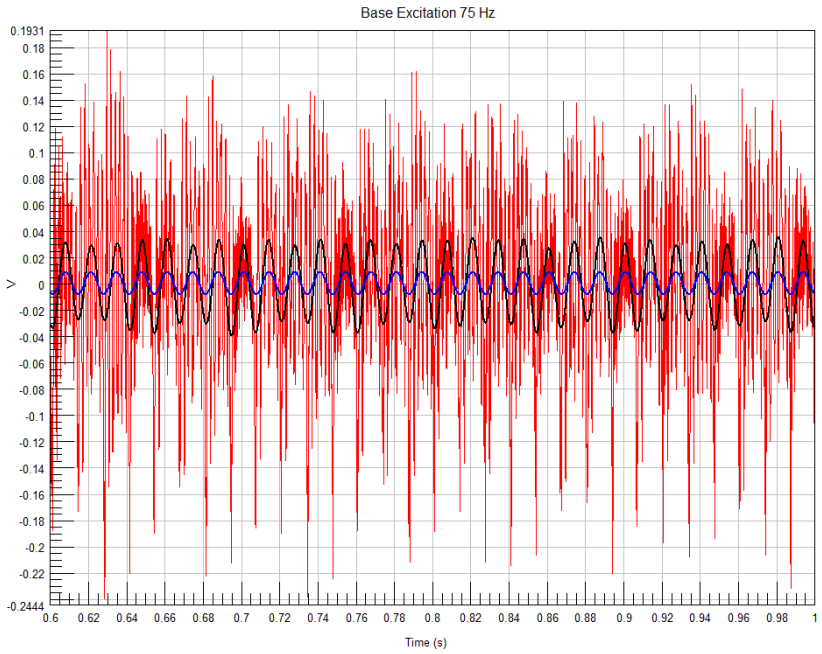

Figure 61. Piezoelectric Material Voltage Outputs at 70 Hz; Blue: without impact, Red: with impact, Black: with impact and 100 Hz low pass-filtered.

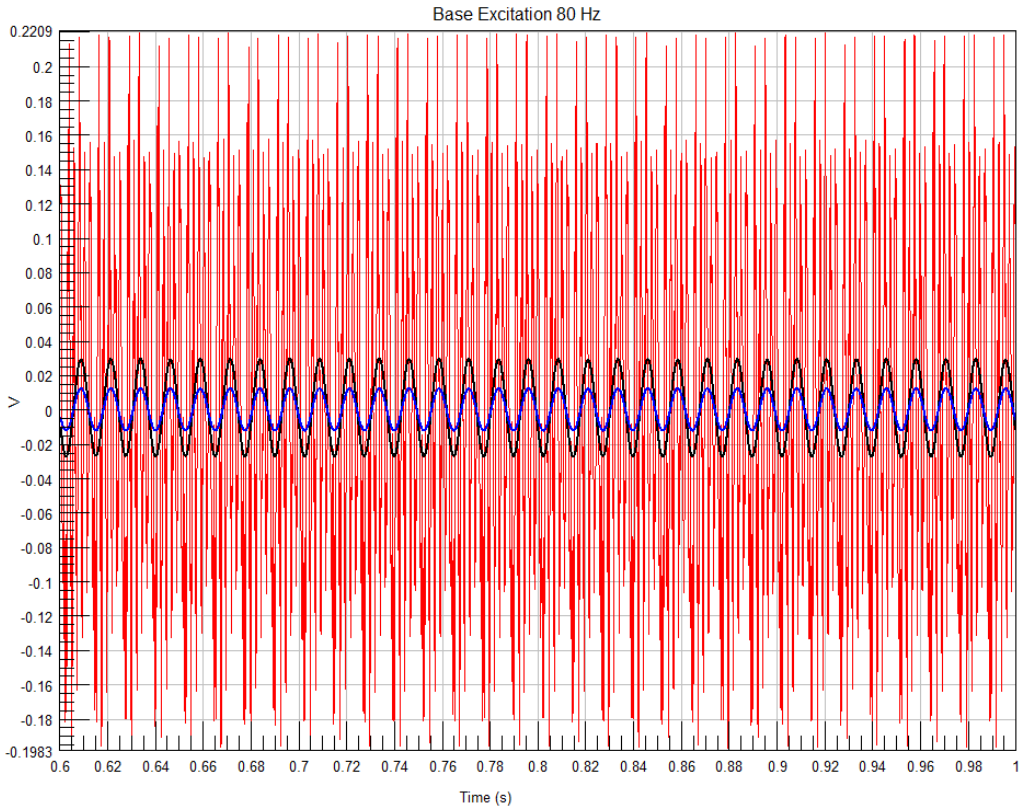

Figure 62. Piezoelectric Material Voltage Outputs at 80 Hz; Blue: without impact, Red: with impact, Black: with impact and 100-Hz low pass-filtered.

Voltage time history graphs given from Figure 53 to Figure 62 are composed of impacting and non-impacting experiments. For the impact condition, measured data is also filtered an 8th order, digital Butterworth low pass with a cut off frequency of 100 Hz to show main form of the motion. This filtering also yields mean time fluctuation of the voltage production of the impacting conditions as shown in black. This information is very critical for comparison of voltage output efficiency.

When graphs are analyzed, at excitation frequencies of 30, 65, 70, 75 and 80 Hz, 100-Hz low pass filtered impacting voltage outputs are much larger than those without impact conditions. On the other hand, at excitation frequencies of

50 and 56 Hz, non-impacting voltage productions are larger than those of 100-Hz low pass filtered impact condition. At excitations of 40.45Hz and 60 Hz, 100-Hz filtered impact condition and without impact conditions give approximately the same voltages as expected from the nature of the frequency response characteristics (Figure 51). These harmonic tests are performed for the same base excitation levels and therefore, by changing the system characteristics of the harvester, output responses are amplified at some frequencies and attenuated at some other frequencies. These results are also compatible with the frequency response characteristics obtained from the white noise experiment (Figure 51). Voltage production capability of the harvester decreases from 40 Hz to 58 Hz when this figure is investigated in detail. Apart from this range, voltage production capability of the harvester looks like increased as validated by experiments. The higher frequencies from 80 Hz could be validated by using same analogy; however, in this study, higher frequencies are not tested because of the limitations in the accelerometer measurement range. However, the first natural frequency band is validated as the most critical area. Table 4 is summarizing voltage production capability of the harvester at different frequencies in detail.

At each frequency, base excitation levels are kept the same for with or without impact conditions. However, changing the frequency of the harmonic base motion leads to a change in acceleration levels for the same gap size between the stopper and the cantilever beam. Therefore, each test voltage outputs should be evaluated within themselves at a particular frequency. In other words, one must be careful in interpreting voltage outputs at differing frequencies.

Table 4. Voltage Production Capability at Different Frequencies

FREQUECNY	***VOLTAGE CHANGE***
30 Hz	160 % Increase
40 Hz	No Increase
45 Hz	30 % Decrease
50 Hz	53 % Decrease
56 Hz	75 % Decrease
60 Hz	No Increase
65 Hz	50 % Increase
70 Hz	100 % Increase
75 Hz	200 % Increase
80 Hz	200 % Increase

4.4 Effects of Stopper Location on Harvester Efficiency

Impact location of the harvester is another important design criterion and changes can cause alterations in dynamic behaviour of the system. Maximum displacement when impact occurs depends on the location of impact as each location on the harvester beam experiences different motion. As a result of this change, resulting acceleration levels, impact forces and impact velocities are also altered. Therefore, voltage output could be affected in the light of this argument.

In the experiment, the stopper is moved towards the clamped end to validate these arguments for the equal amplitude base excitation and the same gap between the stopper and the cantilever beam. Then, the measured voltage output is accepted as the performance criterion of the harvester.

In Figure 63, blue line shows the voltage output when the distance between the stopper and the clamped base is 60mm and black line indicates the voltage output fluctuation when the distance is 81 mm. The voltage output values show that, when excitation frequency coming from the base excites first natural frequency of the beam, moving stopper towards the clamped end increases the voltage output. Therefore, for excitation of the other bending modes, selection of maximum displacement position for the stopper yields the same kind of results.

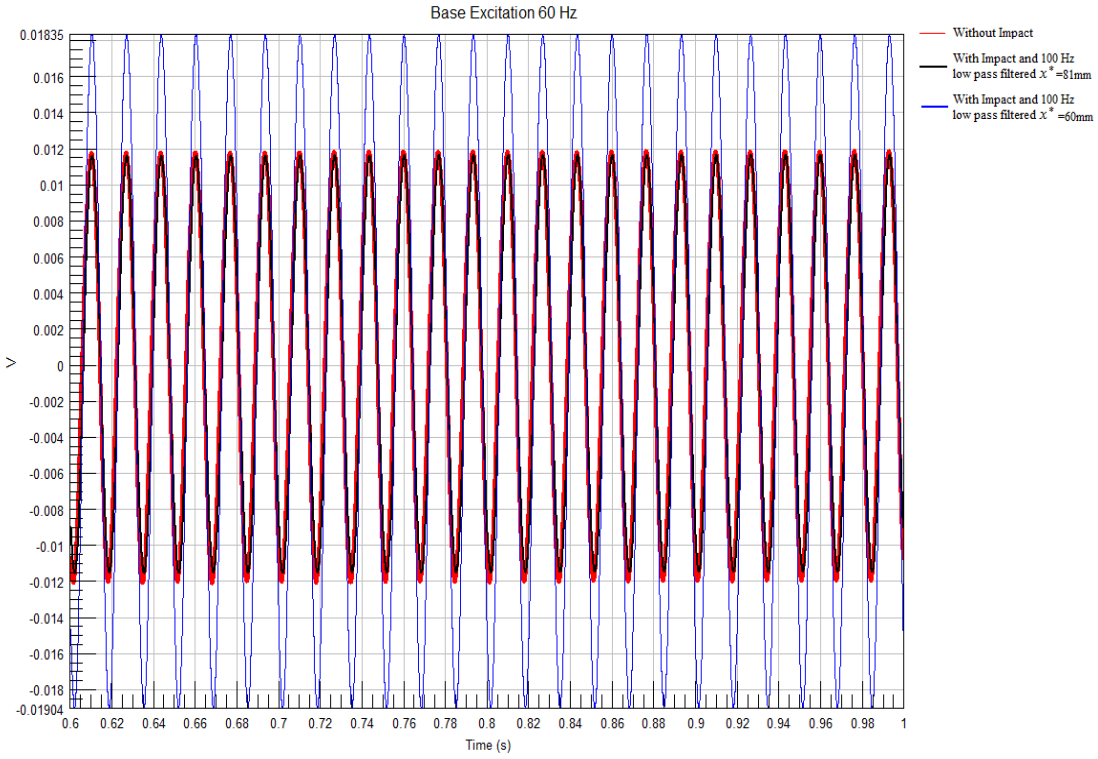

Figure 63. Voltage Output for Different Stopper Location with a Base Excitation Frequency of 60 Hz.

4.5 Leakage Resistance and Capacitance Measurement

In the measured and predicted voltage signals from the theoretical model shows differences due to internal resistance and capacitance of stacks. Therefore, in analytical solution case, losses during incurred in measurement should be in included in models developed. Theoretical values of leakage resistance and capacitance are also derived, however; to validate test results, accurate measurement of these properties is essential. An external resistance is connected to the piezoelectric material to measure leakage resistance and external power supplied to the system. The input voltage and piezoelectric material voltage is measured. Leakage resistance can be found by using calculation given in Figure 64. Figure 68 in the Appendix-B shows the leakage resistance measurement. Through power supply, a constant voltage 8V is supplied to the circuit and an output voltage of 5.9 V is measured. Known resistance value is 3.8 mega-ohms; therefore, leakage resistance is obtained as 14.1 mega-ohms.

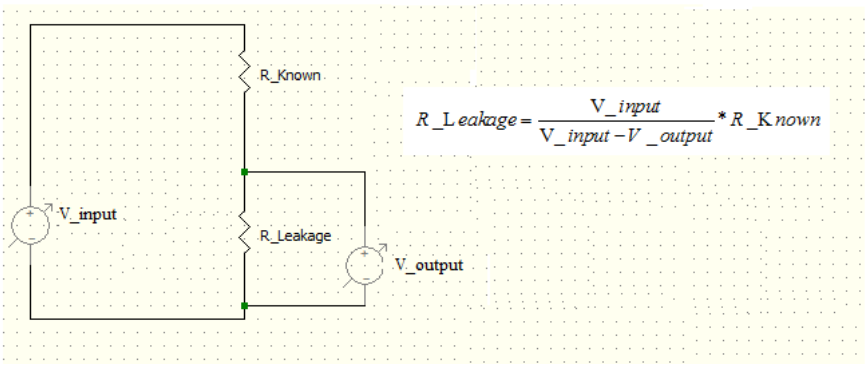

Figure 64. Schematic View of Leakage Resistance Measurement

Capacitance is also measured simply by a multi-meter and 385nF is obtained.

CHAPTER 5

SUMMARY AND CONCLUSIONS

5.1 Summary and Conclusions

The work by Ibrahim *et al*. [1] discusses the importance of having energy harvesters designed to operate at the natural frequency in order to achieve high power outputs. Furthermore, Tang *et al*. [28] show that small deviations in excitation frequency from the natural frequency result in excessive loss of power output. In this study, it was aimed to increase the frequency bandwidth of the energy harvester, which enables to use the harvester in broadband loading environments. In order to achieve this goal, an energy harvester which consists of a cantilever beam with a piezoelectric stack located at its tip and impacting onto a motion stopper is designed.

The cantilever beam naturally amplifies the input at its resonance frequencies. However, as the damping is very small the bandwidth of energy generation is fairly limited. The motion stopper included in the design eliminates this handicap in two ways. Firstly, the impacts generate various harmonics which are instrumental in enrichment the frequency content. Secondly, as the motion stopper transforms the linear system to a nonlinear one, frequency shifts occur as discussed in Chapter 4. However, this modification has also a disadvantage, which is the loss of response amplitude at the resonant frequencies since the motion is disturbed by the stopper.

Linearized response is calculated in this study, although the response of the impacting beam is nonlinear. In order to obtain this linearized response,

undamped response under base excitation is found. The undamped responses are obtained by expansion theorem where the first 5 modes are included. Furthermore, damping ratios for the first 5 natural frequencies are obtained from harmonic tests and damped responses are modified using these values.

Moreover, impact forces are calculated by iteratively solving the coupled dynamic equations of the beam and stopper. If the beam motion overlaps the stopper motion, their coupled responses are solved and impact force developed is calculated. In the next time step, responses of bodies are recalculated using the calculated impact force, provided that it is checked whether they are still in contact or not. Time step in the study is found to be a very important parameter in the solution process to obtain accurate responses. If it is too long, coupled response solution yields very high impact forces and the solution diverges after a few steps. Thus, choose of a time step which is at least equal to six times longer than period corresponding to the highest natural frequency gives accurate results [31]. In this study, time step equal to ten times of the period corresponding to the highest natural frequency is used. In order to obtain an accurate time step value converges studies should be performed.

Validation of the analytical results obtained in Chapter 3 is performed by experiments detailed in Chapter 4. In the first experiment, measured tip mass acceleration is integrated twice to obtain tip displacement of the cantilever beam. Prior to the integrations, acceleration signal are high-pass filtered using an eight order Butterworth filter with a cut off frequency of 10 Hz to remove the mean value and or fluctuations at low frequencies. As the first natural frequency of the cantilever beam is about 60 Hz, using a cut off frequency of 10 Hz does not result in any critical losses for displacements. In the experiments involving impacts high frequency components are observed on the in total response. These high frequency components are expected since impacts generate sub and super harmonics of the excitation frequency due to its

nonlinear nature. However, harmonic responses are found to very low in amplitude compared to the base excitation and impact response. As the theoretical approach used in this study is linear, harmonic effects are not observed in analytical results.

In the experiments, different harmonic excitation at different frequencies and random excitation are applied to the test setup at its based. Firstly, white noise is applied to the harvester for impact and not impact case at the same level and frequency response characteristics of the harvester is obtained. The frequency response characteristic plots show that, impacting beam has higher amplitude up to 1 kHz apart from 35 to 58 Hz band. For validation study, harmonic excitation is given to the harvester from 30 Hz to 80 Hz with 5Hz steps. Results show that, harvested voltage increases with impact for the frequency ranges of 30 to 35 Hz and 58 to 80 Hz while decreases for the frequency range of 40 to 58 Hz. The frequency response characteristic is verified by this method adopted. The impact restricts the motion of the beam which causes a decrease in amplitude at the natural frequency, accompanied by an increase in the bandwidth of the natural frequency. Therefore, this leads to a decrease in harvester efficiency at the first natural frequency. However, the efficiency is shown to increases for the rest of the frequency bandwidth.

Furthermore, the effects of stopper location on harvested energy output are investigated. The stopper restricts the motion of the beam which reduces the amplitude of the response at the first natural frequency, but it increases the amplitude of the response for the rest of the bandwidth. In order to improve the response of the beam at the first natural frequency, the stopper is moved inwards to the clamped end, which will allow the tip to vibrate freely. As the beam still impacts, the positive contributions are still available for harvesting. It is observed that positioning the stopper close to the clamped end increases the voltage output of the harvester compared to the tip mass location for the

same at first natural frequency excitation. Thus, this outcome shows that there is a need to optimize the location of the stopper.

Consequently, it can be said that the proposed energy harvester has a promising potential for engineering applications, but still open to further improvements.

5.2 Recommendations for Future Work

There still exist several aspects that need further investigation though several parameters concerning energy harvesting are investigated in this study. Possible future work is listed as:

i) Nonlinear effects concerning harmonics generated may be included in analytical solution process.

ii) Optimization studies for the stopper location and gap can be conducted to maximize the energy harvested.

iii) Improvements on the impacting beam concerning different designs such as double impacting or having different boundary conditions can be investigated.

iv) Finally, different impacting geometries such as plates can be investigated.

REFERENCES

[1] S.W. Ibrahim, W.G. Ali, A Review on Frequency Tuning Methods for Piezoelectric Energy Harvesting Systems, Journal of Renewable and Sustainable Energy 4 (2012) 062703.

[2] C.B. Williams, R.B. Yates, Analysis of a Micro-electric Generator for Microsystems, Sensors and Actuators A 52 (1996) 8-11.

[3] P. Mitcheson, P. Miao, B. Start, E. Yeatman, A. Holmes, T. Green, MEMS Electrostatic Micro-Power Generator for Low Frequency Operation, Sensors and Actuators A 115 (2004) 523-529.

[4] S. Roundy, P. Wright, J. Rabaey, Energy Scavenging for Wireless Sensor Networks, Kluwer Academic Publishers, Boston, (2003).

[5] S. Roundy, P.K. Wright, J.M. Rabaey, A study of Low Level Vibrations as a Power Source for Wireless Sensor Nodes, Computer Communications 26 (2003) 1131-1144.

[6] J. Rastegar, R. Murray, C. Pereira, H.L. Nguyen, Event Sensing and Energy Harvesting Power Sources for Gun Fired Munitions, Proc. of SPIE Vol.7288 72880Z-1.

[7] Noliac Systems, Last accessed May 21, 2014, http://www.noliac.com/Sensors_transducers.pdf.

[8] APC International Ltd. Last accessed May 23, 2014, http://www.americanpiezo.com/piezo_theory/piezo_theory.pdf.

[9] K. Ersoy, Piezoelectric Energy Harvesting for Munitions Applications, MSc. Thesis in Mechanical Engineering, Middle East Technical University, 2011.

[10] S.R. Pearson, Modeling and Development of Piezoceramic Energy Harvester for Munitions Applications, MSc. Thesis in Electrical Engineering, Villanova University, 2006

[11] A. Ertürk, Electromechanical Modelling of Piezoelectric Energy Harvester, Ph.D. Thesis in Engineering Mechanics, Virginia Polytechnic Institute and State University, 2009

[12] V. Leonov, R.J.M. Vullers, Journal of Renewable Sustainable Energy 1 (2009), 043105

[13] X. Wu, J. Lin, S. Kato, K. Zhang, T. Ren, L.Liu, A Frequency Adjustable Vibration Energy Harvester, in Proceedings of PowerMEMS, Sendai, Japan, 2008.

[14] C. Eichhorn, F. Goldschmidtboing, P. Woias, A Frequency Tunable Piezoelectric Energy Converter Based on a Cantilever Beam, Proceedings of PowerMEMS , Sendai, Japan, 2008

[15] C. Eichhorn, F. Goldschmidtboing, P. Woias, Journal of Micromechanics and Microengineering 19 (2009), 094006.

[16] V.R. Challa, M.G. Prasad, Y. Shi, F.T. Fisher, A Vibration Energy Harvesting Device with Bidirectional Resonance Frequency Tunability, Smart Materials and Structures 17(1) (2008), 015035

[17] V.R. Challa, M.G. Prasad, F.T. Fisher, High Efficiency Energy Harvesting Device with Magnetic Coupling for Resonance Frequency Tuning, Proceedings in SPIE 6928, 692805, 2008.

[18] C. Peters, D. Maurath, W. Schock, and Y. Manoli, Novel Electrically Tunable Mechanical Resonator for Energy Harvesting, Proceedings of PowerMEMS , Sendai, Japan, 2008

[19] M. Lallart, S.R. Anton, D.J. Inman, Journal of Intelligent Material Systems and Structures 21(9) (2010), 897-906.

[20] K.H. Mak, S. McWilliam, A.A. Popov, C.H.J. Fox, Performance of a Cantilever Piezoelectric Energy Harvester Impacting a Bump Stop, Journal of Sound and Vibration 330 (2011), 6184-6202.

[21] C. Wang, J. Kim, New Analysis Method for a Thin Beam Impacting Against Stop Based on the Full Continuous Model, Journal of Sound and Vibration 191(5) (1996), 809-823

[22] A. Rysak, M. Müller, M. Borowiec, J. Zubrzycki, G. Litak, Energy Harvesting in a Beam With Impacts: Experimental Studies, Proceedings Polish National Science Center, Lublin, Poland.

[23] L. Meirovitch, Fundamentals of Vibrations, McGraw-Hill International Edition 2001, 189-198.

[24] S.J. Ahn, W.B. Jeong, W.S. Yoo, Improvement of Impulse Response Spectrum and Its Application, Journal of Sound and Vibration 288 (2005), 1223-1239.

[25] Noliac Systems, Last accessed May 21, 2014, http://www.noliac.com/Energy_Harvesting.pdf.

[26] K.H. Mak, S. McWilliam, A.A. Popov, C.H.J. Fox, Vibro-Impact Dynamics of a Piezoelectric Energy Harvester, Proceedings of the IMAC 28, Jacksonville, Florida, USA 2010.

[27] D. Arnold, Review of Microscale Magnetic Power Generation, IEEE Transactions on Magnetics 43, 3940-3951

[28] L. Tang, Y. Yang, C.K. Soh, Toward Broadband Vibration-based Energy Harvesting, Journal of Intelligent Material Systems and Structures 21 (18) (2010), 1867-1897

[29] A Fathi, N. Popplewell, Improved Approximations for a Beam Impacting Stop, Journal of Sound and Vibration 170(3), 365-375

[30] D.J. Wagg, G. Karpodinis, S.R Bishop, An experimental Study of the Impulse Response of a Vibro-Impacting Cantilever Beam, Journal of Sound and Vibration 228(2) (1999), 243-820

[31] C. C. Lo, A Cantilever Beam Chattering Against a Stop, Journal of Sound and Vibration 69(2) (1980), 245-255

[32] Noliac Systems, Last accessed July 8, 2014, http\\www.noliac.com_Specifications-141.pdf

[33] Micromechatronics Inc.(MMech) ,Last accessed July 8, 2014, http://www.mmech.com/index.php?option=com_content&view=article&id=110&Itemid=339

[34] W.J Palm, Mechanical Vibration, John Wiley and Sons, New York 2006.

APPENDIX- A

PIEZOELECTRIC MATERIAL PROPERTIES

Piezo materials specification
Standard product

Properties	Symbol & unit	NCE40	NCE41	NCE46*	NCE51	NCE53	NCE55	NCE56	NCE57*	NCE59*	NCE80
DIELECTRIC PROPERTIES (tolerances +/- 10%)											
Relative Dielectric Constant	ε^T_{33} / ε_0	1250	1350	1300	1900	1600	5000	2900	1800	2900	1050
Dielectric Loss Factor	tgδ [10^{-4}]	25	40	30	150	130	220	140	170	190	20
Dielectric Loss Factor at 400V/mm	tgδ [10^{-4}]	140	200								100
ELECTROMECHANICAL PROPERTIES (tolerances +/- 5%)											
Electromech. Coupling Factors**	k_p	0.58	0.57	0.57	0.65	0.56	0.62	0.64	0.59	0.64	0.55
	k_{31}	0.34	0.33	0.33	0.38	0.32	0.39	0.37	0.33	0.37	0.30
	k_{33}	0.70	0.68	0.68	0.74	0.65	0.72	0.74	0.70	0.75	0.68
	k_t	0.50	0.50	0.47	0.50	0.47	0.50	0.50	0.47	0.52	0.48
Piezoelectric Charge Constants	$-d_{31}$ [10^{-12} C/N]	140	130	130	195	150	260	250	170	240	100
	d_{33} [10^{-12} C/N]	320	310	330	443	360	670	580	425	575	240
Piezoelectric Voltage Constants	$-g_{31}$[10^{-3} Vm/N]	11	11	11	13	9	9	9	11	10	11
	g_{33} [10^{-3} Vm/N]	27	25	28	26	23	19	20	27	23	27
Frequency Constants	N^E_p [m/s]	2160	2280	2230	1925	2180	1970	2000	2010	1970	2270
	N^D_t [m/s]	1980	2000	2040	2000	2040	1990	2030	1950	1960	2050
	N^E_1 [m/s]	1470	1600	1500	1370			1530	1400	1410	1610
	N^D_3 [m/s]	1340	1500	1800	1320			1400	1500	1500	1500
PHYSICAL PROPERTIES (tolerances +/- 5%)											
Mechanical Quality Factor	Q_m	700	1400	>1000	80	80	70	80	80	90	1000
Density	ρ [10^3 kg/m^3]	7.75	7.9	7.7	7.85	7.6	8	7.65	7.7	7.45	7.8
Elastic Compliances	s^E_{11} [10^{-12} m^2/N]	13	13	13	16	16	17	18	17	17	11
	s^E_{33} [10^{-12} m^2/N]	17	16	20	19	18	21	20	23	23	14
Curie Temperature	T_C [°C]	318	284	330	360	340	159	242	350	235	307

*) For multilayer components only.
**) Measured in accordance with standard EN 50324.

Figure 65. CMAR03 material properties for NCE57 ceramics [32].

Product facts:

CMAR03	Value	Tolerance
Length/outer diameter	12 mm	± 0.40 mm
Width/inner diameter	6 mm	± 0.20 mm
Height	2 mm	± 0.05 mm
Operating voltage	200 V	
Free stroke	2.8 µm	± 15%
Blocking force	2670 N	± 20%
Capacitance	350 nF	± 15%
Stiffness	950 N/µm	± 20%
Maximum operating temperature	200 °C	
Curie temperature	350 °C	
Material	NCE57 (S1)	
Unload resonance frequency	> 500 kHz	
External electrodes	Screen-printed Ag or Ag/Pd	
Wires	Optional	

Typical outline:

The figure below shows typical outline of CMAR's

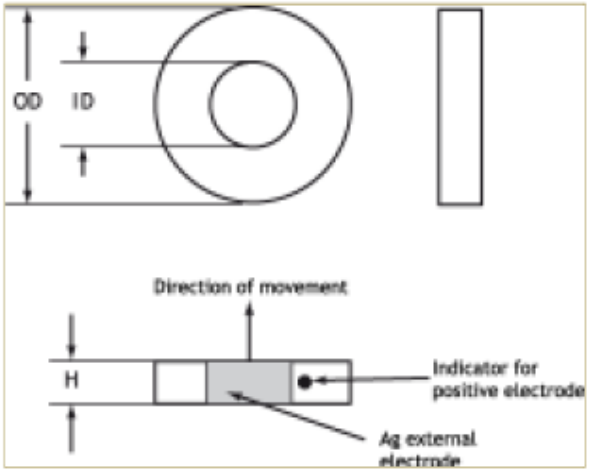

Symbol	Parameter	Unit
OD	Outer diameter excluding external connections	mm
ID	Inner diameter	mm
H	Height	mm

Figure 66. Physical properties for CMAR03 piezoelectric properties[33].

APPENDIX- B

B. PIEZOELECTRIC MATERIAL CONSTANTS

Table 1 – Piezoelectric Material Constants	
Piezoelectric Constant	Description
ε_r	Relative Dielectric Constant • Used in calculating the capacitance of the material
tan δ	Loss Tangent • A frequency dependent ratio between the real and imaginary parts of the impedance of a capacitor. • A large dielectric constant implies a lot of dielectric absorption [7]
k_{ij}	Coupling Coefficient • A measure of the coupling between the mechanical energy converted to electrical charge, and the mechanical energy input
D_i	Electric Displacement • Dielectric constant times the electric field
d_{ij}	Piezoelectric Constant (C/N) • The piezoelectric charge coefficient is the ratio of electric charge generated per unit area to an applied force [5]
g_{ij}	Piezoelectric Voltage Constant (Vm/N) • The voltage constant is equal to the open circuit field developed per unit of applied stress, or as the strain developed per unit of applied charge density or electric displacement [8]
e_{ij}	Piezoelectric Modulus (C/m^2) • The ratio of strain to applied field, or charge density to applied mechanical stress [8]
N_i	Frequency Constant (m/s) • The frequency constant is the product of the resonance frequency and the linear dimension governing the resonance. [9]
Q_m	Quality Factor • Measure of how well a system will resonate at or close to its resonance frequency [6]
ρ	Density (kg/m^3) • Ratio of mass to volume
σ^E	Poisson's Ratio • A measure of how, when a material is stretched in one direction, it becomes thinner in the other two [6]
s^a_{ij}	Elastic Compliance (m^2/N) • The inverse to Young's Modulus • Ratio of mechanical strain to stress [9]
Y^a_{ij}	Young's Modulus (Pascals) • Ratio of mechanical stress to strain

Figure 67. Piezoelectric Material Constants

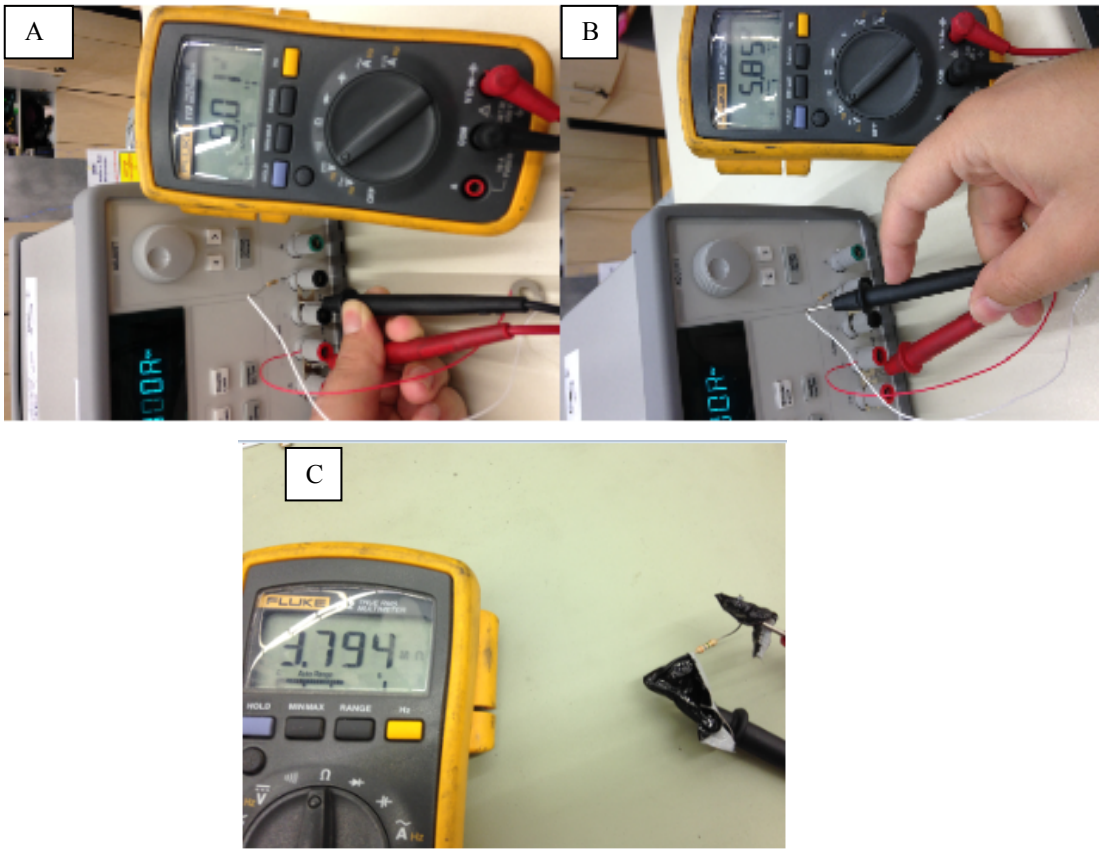

Figure 68. Leakage Resistance Measurement, A- V_input Calculation, B- V_output Calculation, C- Resistance Measurement Known Resistance.

Figure 69. Capacitance Measurement of Piezoelectric Material